Sensor and Simulation Notes

Note 236

11 November 1977

The Dipole Method (DIES) in SGEMP Simulation

G. A. Seely
Science Applications, Inc.
2201 San Pedro, NE
Albuquerque, New Mexico 87110

Abstract

Some of the practical aspects of this source current replacement-simulation technique are examined. A method is described for combining experimental dipole data with calculated SGEMP volume currents. The results for a limited parameter variation concerning the requisite antenna grid are reported.

CONTENTS

ILLUSTRATIONS

Illustrations (continued)

SECTION I

INTRODUCTION

The system-generated electromagnetic pulse (SGEMP) effects on a satellite may prove to be the dominant effects governing satellite survival and yet these effects are not well understood. There is, at present, no simulation facility which can realistically simulate the satellite environment, to excite a complete satellite. Consequently, other techniques must be used in the interim to investigate the complicated phenomenon created by electron emission from the surface of a satellite.

A novel technique has recently been suggested by Baum (References 1 and 2). The basic simulation scheme involves measuring a transfer function between an infinitesimal current element outside the system under test and a critical circuit element buried within the system. Using calculated SGEMP volume currents, weighted integrals of the transfer functions and the volume currents yield the total SGEMP response at the circuit level.

In effect, the technique attempts to take advantage of the better aspects of the two methods. The electrical response of the interior of a large complicated system is at present better determined by measurement. The exterior problem, on the other hand, is presently more amenable to analysis using existing SGEMP codes.

Several potential obstacles to implementing this technique immediately come to mind. Upon closer examination it becomes apparent that most of those are closely related to a single parameter: the number of dipole positions required to accurately simulate the external environment.

For example, the most widely used electromagnetic pulse (EMP) simulators (i.e., ALECS, ARES, TEMPS, SIEGE, RES, TORUS, ACHILLES, ATHAMAS, ...) are, this context, single source simulators. That is, the source doesn't change during the test (although a few penetrations may be driven concurrently with the test). With the dipole method, several antenna positions would be required, with data taken at each antenna position.

The time and cost for the measurement of responses on the satellite for many dipole volume elements can be circumvented to some extent by using automated recording instrumentation such as ABACIS* and by constructing an automated device for moving and positioning the dipole antennas.

This, however, is not the total answer. The potential for error goes up rapidly with an increase in the volume of data handled. If many measurements are required, system checks and assurance of data quality suffer by the sheer time and cost limitations imposed by the need for such a large amount of data. If a large volume of data is required, then potential errors in the instrumentation system and errors in annotating the data may not be caught until the test is over, the system dismantled, and everyone has gone home.

A fine grid detail would necessitate the use of very small dipole antennas. As size goes down, it is generally true that signal/noise problems increase which can make it difficult to obtain reliable data. Transmitters, power supplies and other equipment associated with the dipole antenna would have to be scaled down accordingly for an equivalent quality of data. This problem is compounded by the rapid variation in both space and time (frequency) in the near field of a dipole antenna. Equipotentials are not available for positioning of transmitters or for cable routing from the antenna.

An actual satellite would be tested in a finite facility in which nearby objects and the earth could behave as reflectors and thereby degrade the quality of the simulation. For the close-in antenna positions, these effects can be made small. This is not the case, however, for more distant measurements. Not only does the signal/noise go down, the reflections can become as large as the desired measurement. Thus, a need exists, in some fashion, to limit the volume size required for the simulation and, if possible, to take into account the more distant currents.

*Autonetics Broadband Automatic Calibrated Instrumentation System. This continuous-wave system outputs magnetic tape and avoids the necessity of digitizing the experimental data.

The requirements on the quality of the experimental data and the calculated SGEMP currents increase as the number of measurements increase. The technique for combining the analytical and experimental data would have to be both accurate and efficient. This is particularly true if continuous-wave data is recorded, since Fourier transforms and/or inverse transforms would be required to combine the results.

Further examples could be given, the conclusion would be the same. The number of measurements required to accurately simulate the external environment is the single most important parameter impacting the practicality of the dipole method. In detail, this depends on its implications concerning volume size required for simulation, grid detail for antenna placement, antenna size, requirements on the quality of the SGEMP currents, the experimental data and the quality of the combining technique.

In view of these considerations, an effort was undertaken to provide preliminary data concerning these constraints. For the results to be specific, a single two-dimensional test object was selected for treatment in the bulk of the report.

This report is arranged in sections. The test object geometry is described in Section II. The remainder of the report is devoted to a description of the computation techniques, followed by the results and conclusions which are presented in Sections VII and VIII, respectively.

SECTION II

TEST OBJECT DESCRIPTION

The test object chosen for analysis is a right circular copper cylinder with a solder coat sufficiently thick to prevent X-ray transport through the walls of the cylinder. This two-dimensional object retains some of the features of an actual satellite yet with the simplicities inherent in two dimensions. In addition, some experimental and analytical data are available on this test object (References 3 and 4).

For real systems, SGEMP must ultimately couple to interior circuitry to be of concern. The test object has a circumferential aperture and an interior axial post electrically connecting the base and the top of the cylinder. The geometry used for the analysis is shown in Fig. 1.

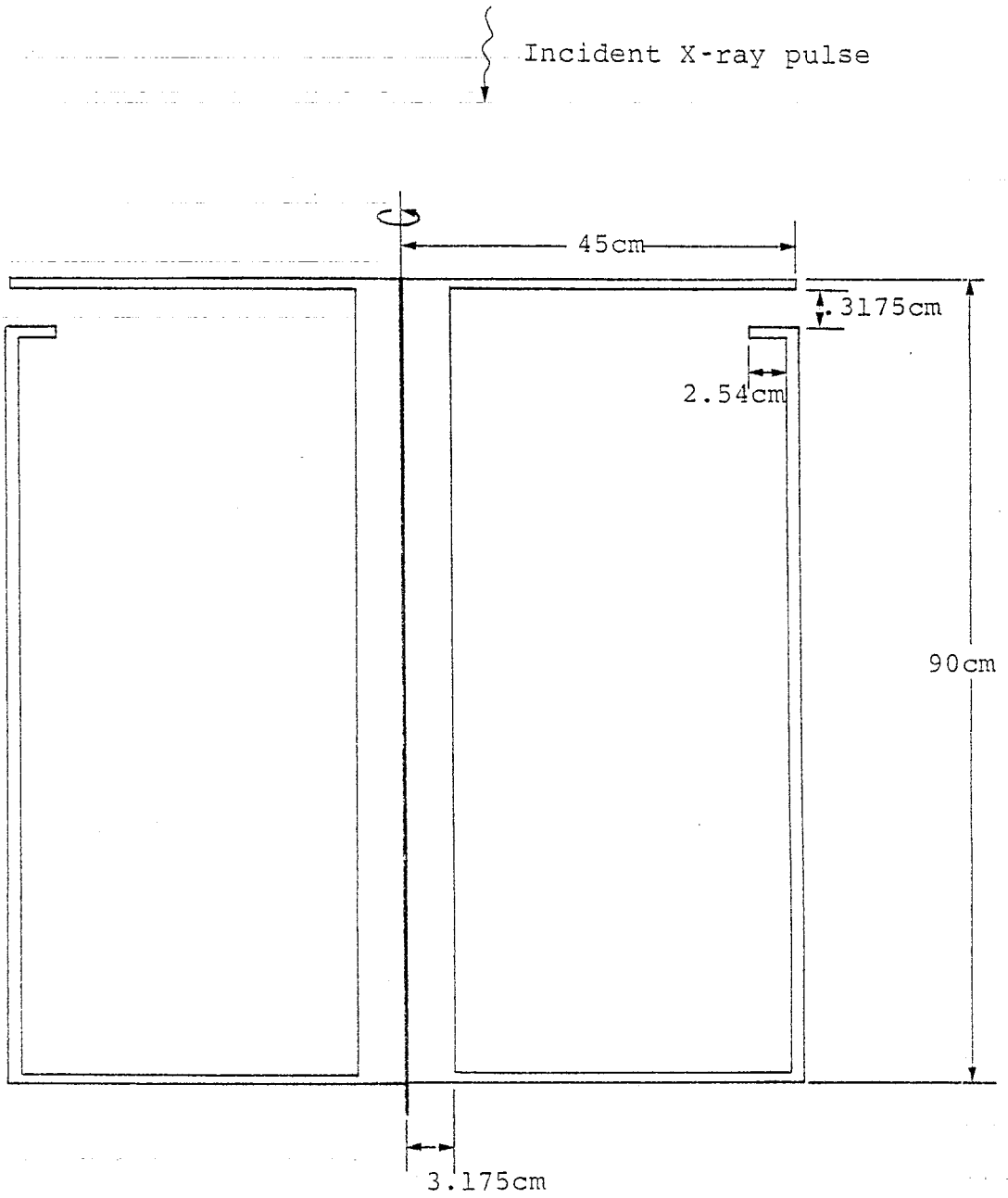

Figure 1. Test Object Geometry.

SECTION III

NUMERICAL METHOD FOR OBTAINING DIPOLE DATA

1. GENERAL

At this stage of the investigation it was convenient to numerically simulate the experimental dipole data. This would provide initial data for use as testing functions for combining techniques, grid detail and volume size without the expense of first doing the experiment. The numerical data could also be retained for later comparison to experimental results, as well as giving some indication of the importance of more distant current elements.

Direct time stepping of Maxwell's equations in two dimensions was chosen as the simplest available technique for obtaining the dipole-satellite interaction functions.

The algorithm is a simplified version of the fields algorithm in the MAD2 SGEMP code (Reference 4). Special use was made of the simplicities introduced by a single dipole source in any one calculation, and by using a uniform grid size. Additional simplifications were made by factoring out constants that occur repeatedly in the calculation.

The cylinder response results for representative dipole locations are described in the following subsection.

2. EXEMPLARY DATA

Figure 2 displays the antenna positions for which data is described in this section. The numbers beside the ring dipoles correspond to the graph numbers for the specific antenna positions and polarizations. In Fig. 2, the z-coordinate is vertically upward and the ρ-coordinate is horizontal. The coordinate origin is located on the center top of the cylinder; a is the cylinder radius (0.45 m).

Table 1 lists the location of the antenna positions corresponding to the graph number. Dimensions are given in units of the cylinder radius a.

TABLE 1

ANTENNA POSITIONS AND POLARIZATIONS
FOR DATA PRESENTED IN SECTION III

Graph No.	Antenna Position z/a	Antenna Position ρ/a	Polarization
2	0.125	0.0	z-directed dipole
4	3.125	0.0	z-directed dipole
6	0.125	0.75	z-directed dipole
15	-0.875	3.50	z-directed dipole
18	3.125	3.50	z-directed dipole
26	0.25	0.125	ρ-directed dipole
28	3.00	0.125	ρ-directed dipole
30	0.25	0.875	ρ-directed dipole
34	-1.00	1.625	ρ-directed dipole
39	-1.00	3.625	ρ-directed dipole
42	3.00	3.625	ρ-directed dipole

Figure 3 displays the time derivative of the antenna dipole moment P used to obtain the results in this section. The peak value of $\dot{P}$ is 1 Am. The time scale ct/a is normalized to the cylinder radius and the speed of light. Thus, when ct/a = 1, the time t is 0.45 m/0.3 ns/m = 1.5 ns.

The time dependence for the antenna dipole moment corresponds to the time dependence for a critically damped series RLC circuit. Although not crucial at this stage, this choice is a reasonable approximation for a realizable pulse-driven small dipole antenna. The 10-90 rise time for the dipole current in Figure 3 is 1 ns.

The locations given for the tangential magnetic HC, HS (Am^{-1}) and normal electric EC, ES (Vm^{-1}) fields are indicated in Fig. 2. The coordinates are given in Table 2.

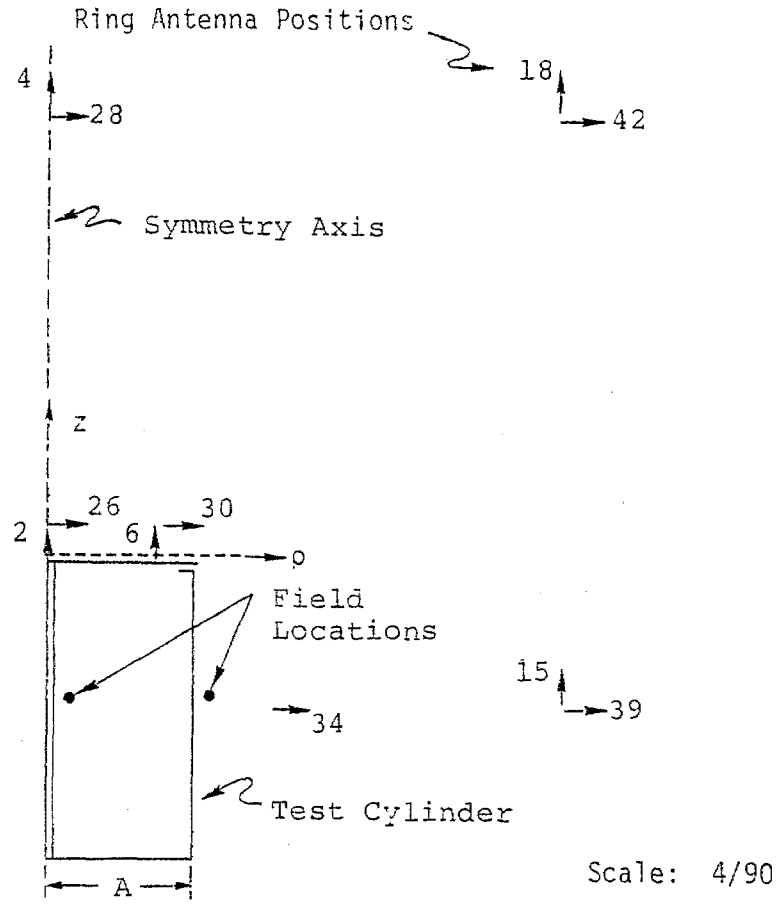

Figure 2. Planar View of 2-D Geometry Showing Dipole Ring Positions.

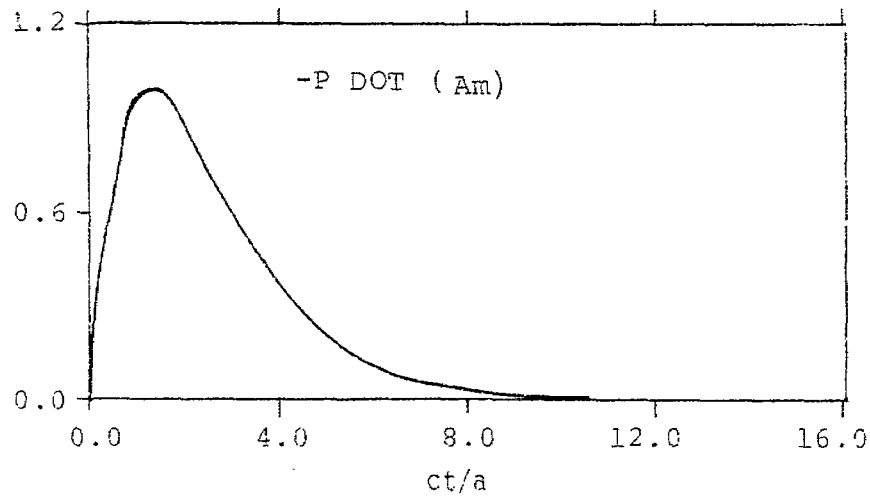

Figure 3. Time Derivative of the Ring Dipole Moments.

TABLE 2

FIELD LOCATIONS FOR DATA
PRESENTED IN SECTION III

Field Component	Location z/a	Location ρ/a
HC (Am^{-1})	-0.875	0.125
EC (Vm^{-1})	-1.0	0.125
HS (Am^{-1})	-0.875	1.125
ES (Vm^{-1})	-1.0	1.125

Figures 4 through 14 display the tangential magnetic field and the normal electric fields for the indicated antenna positions and polarizations.

Data of particular interest is for the antenna position corresponding to graph No. 2 (Fig. 4). This result would provide the simplest comparison to experimental data when it is available.

An additional feature worthy of note is the persistance of the static part of the electric field coupling to the cylinder even for antennas some distance from the cylinder (ES for graph Nos. 4, 15, 28, 39, and 42).

In Fig. 12 (graph No. 34), it is of interest to notice that the normal electric field on the cylinder surface ES is proportional to the antenna's dipole moment (the time integral of PDOT in Fig. 3). This would indicate that at this distance, the normal electric field is dominated by the static field produced by the dipole antenna.

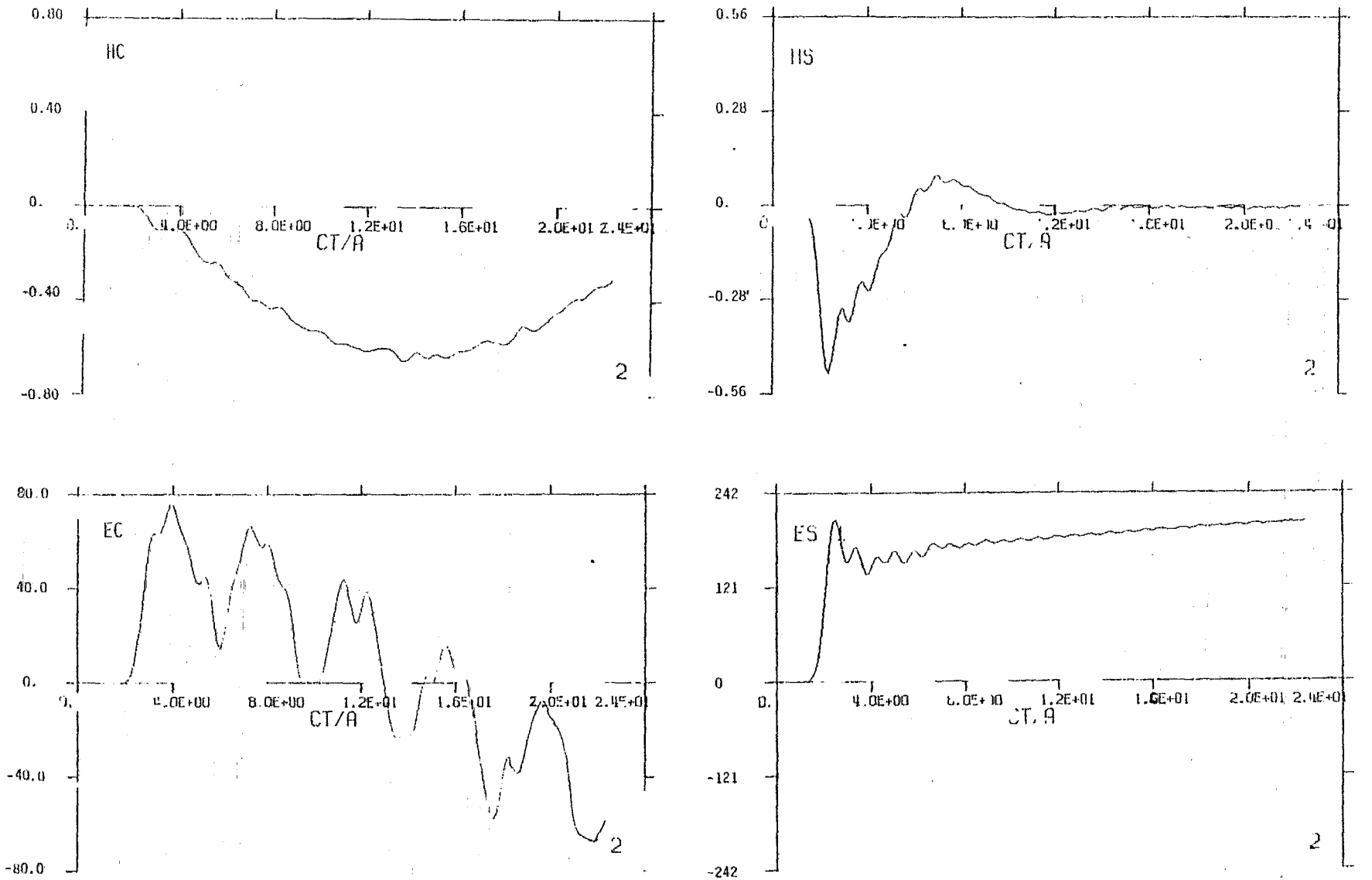

Figure 4. Cylinder Response for z-Directed Ring Dipole at (z/a, ρ/a) = (0.125, 0.0).

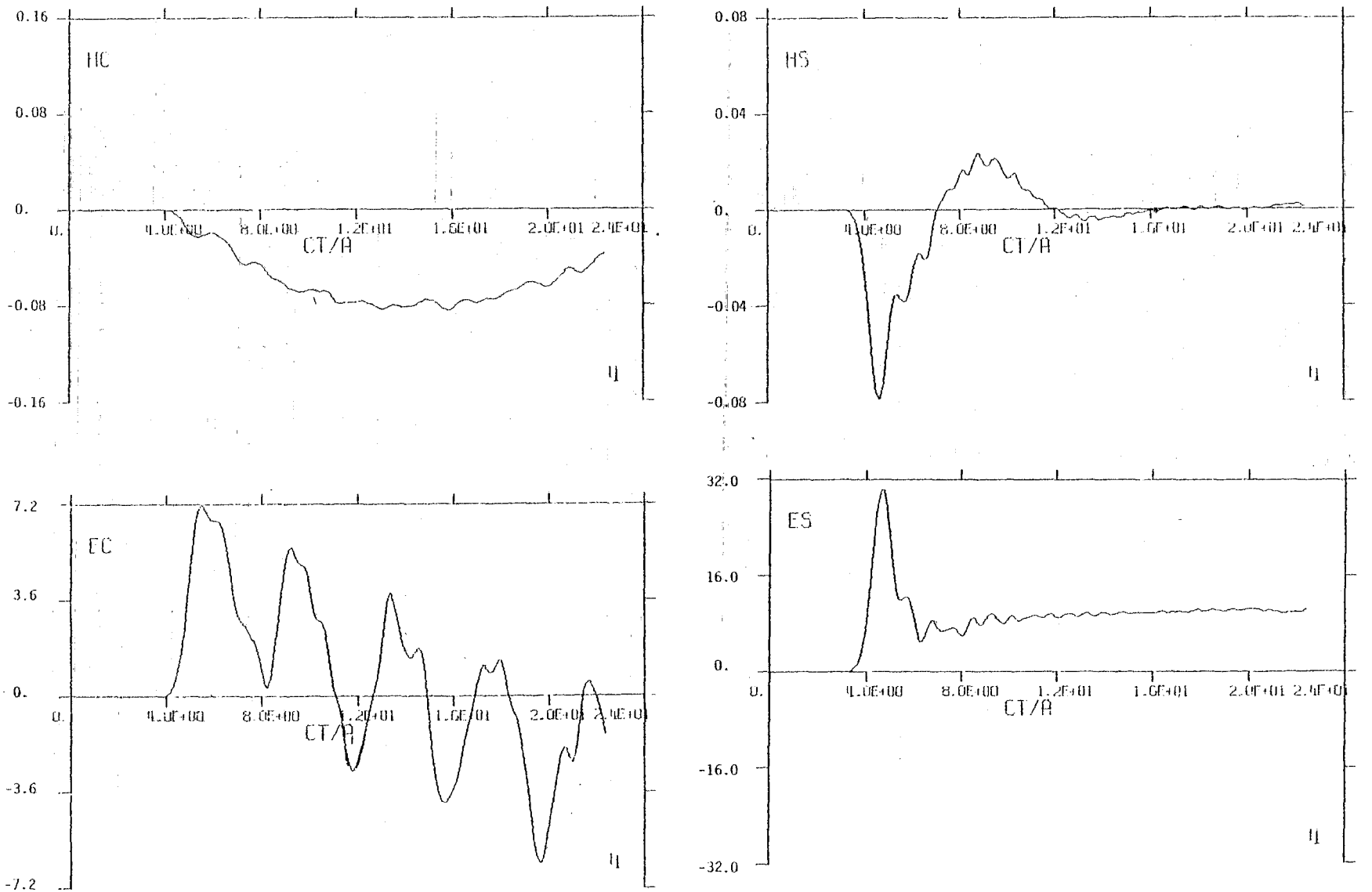

Figure 5. Cylinder Response for z-Directed Ring Dipole at (z/a, ρ/a) = (3.125, 0.0).

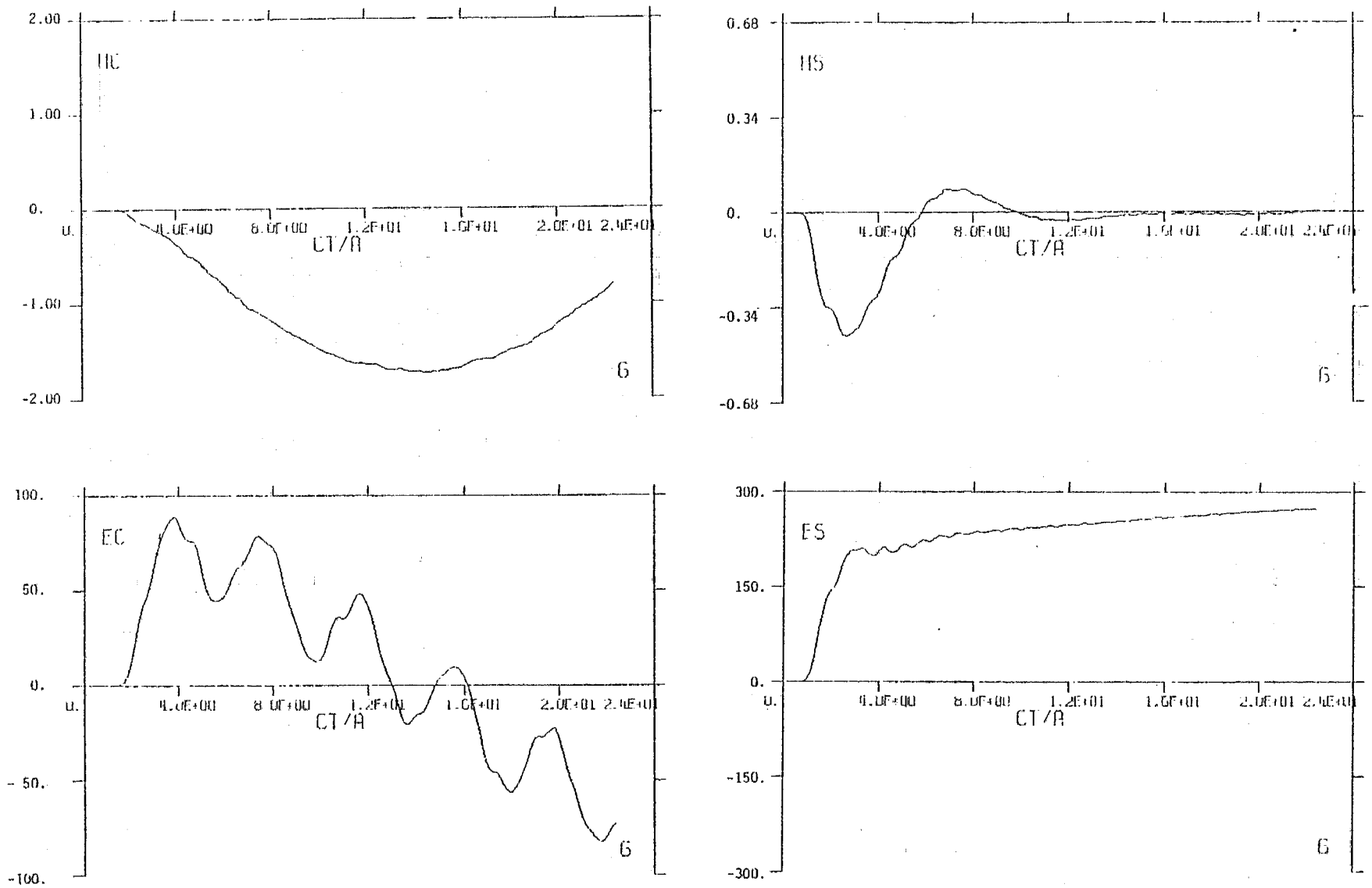

Figure 6. Cylinder Response for z-Directed Ring Dipole at (z/a, ρ/a) = (0.125, 0.75).

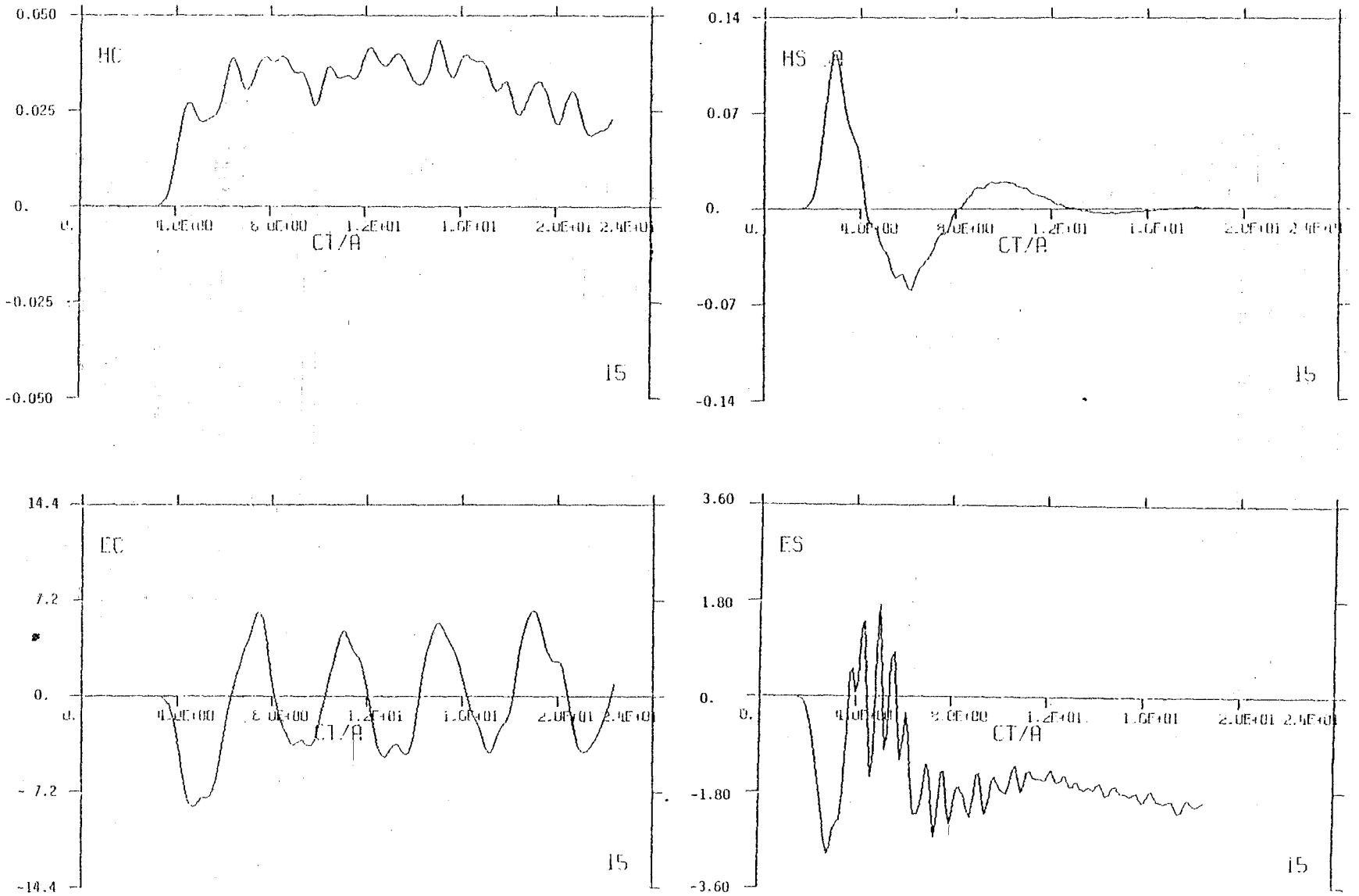

Figure 7. Cylinder Response for z-Directed Ring Dipole at (z/a, ρ/a) = (-0.875, 3.50).

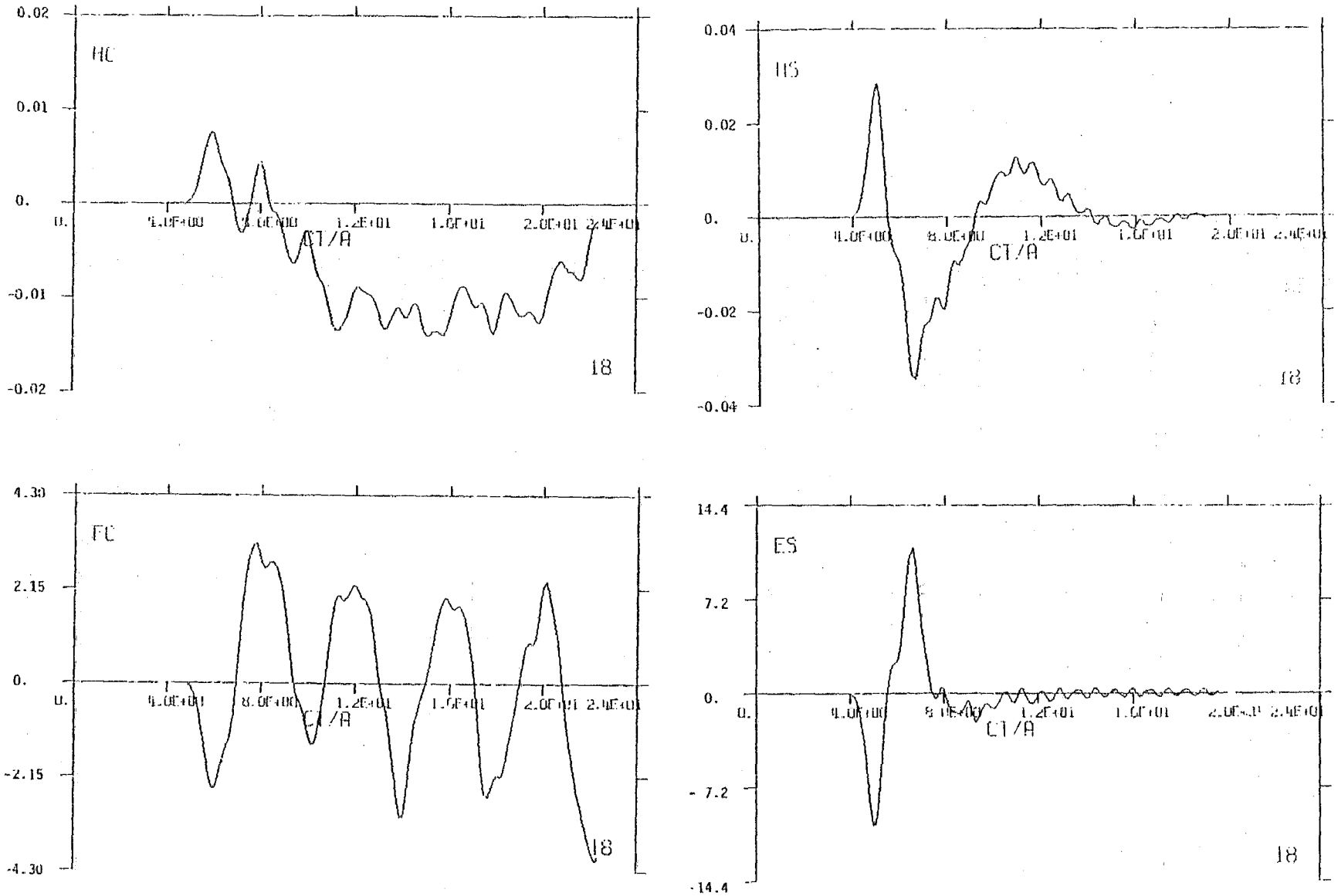

Figure 8. Cylinder Response for z-Directed Ring Dipole at (z/a, ρ/a) = (3.125, 3.50).

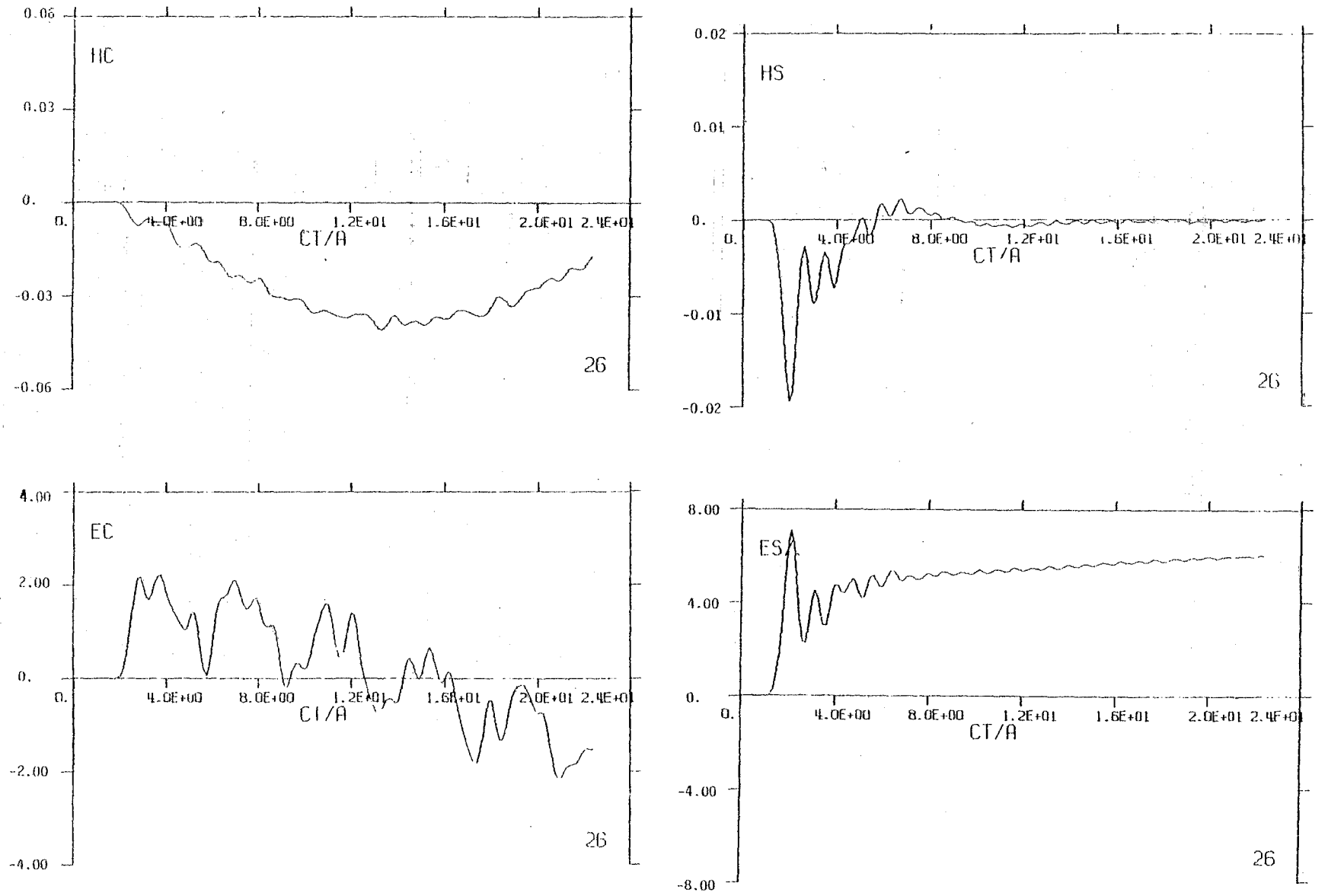

Figure 9. Cylinder Response for ρ -Directed Ring Dipole at (z/a, ρ/a) = (0.25, 0.125).

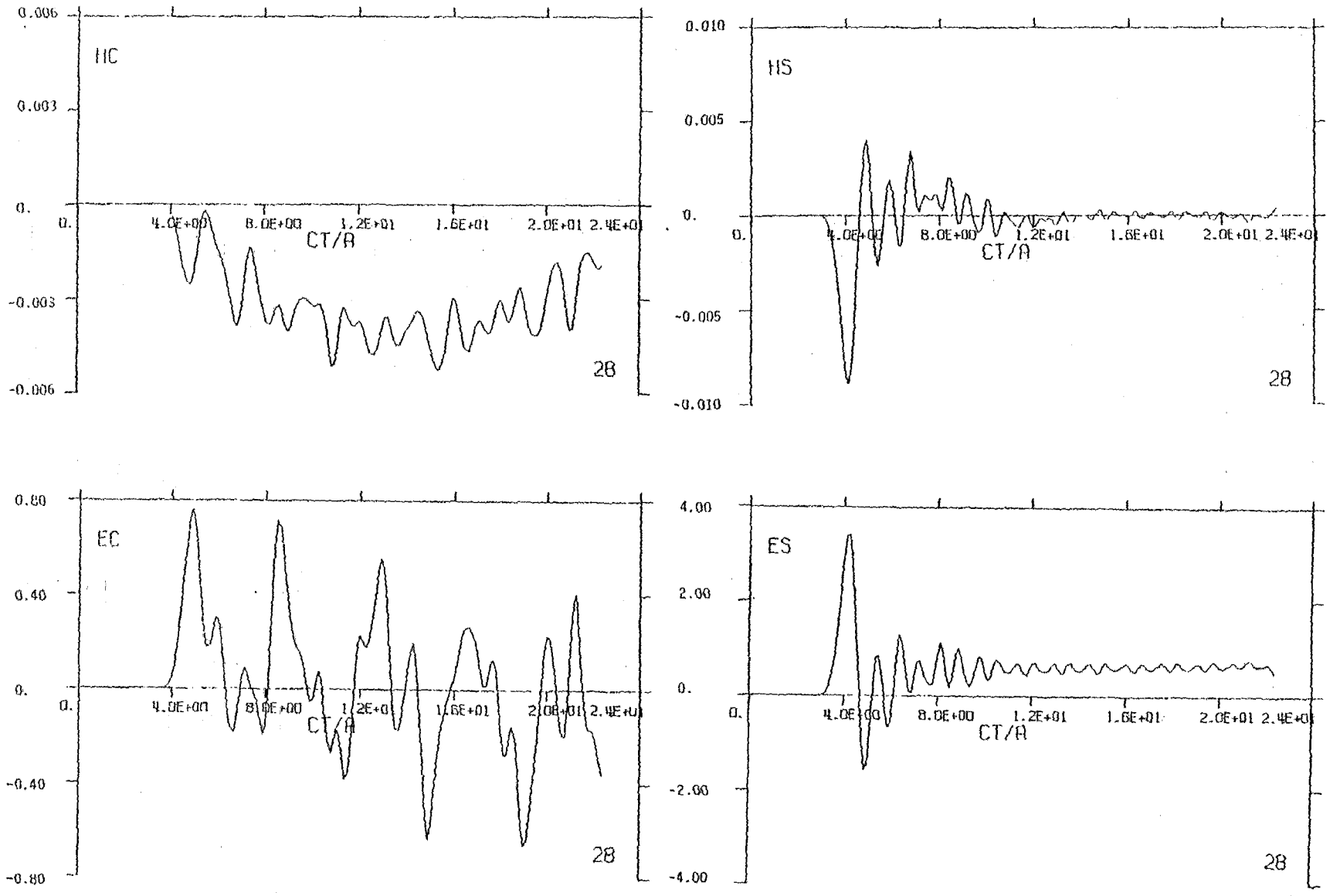

Figure 10. Cylinder Response for ρ-Directed Ring Dipole at (z/a, ρ/a) = (3.00, 0.125).

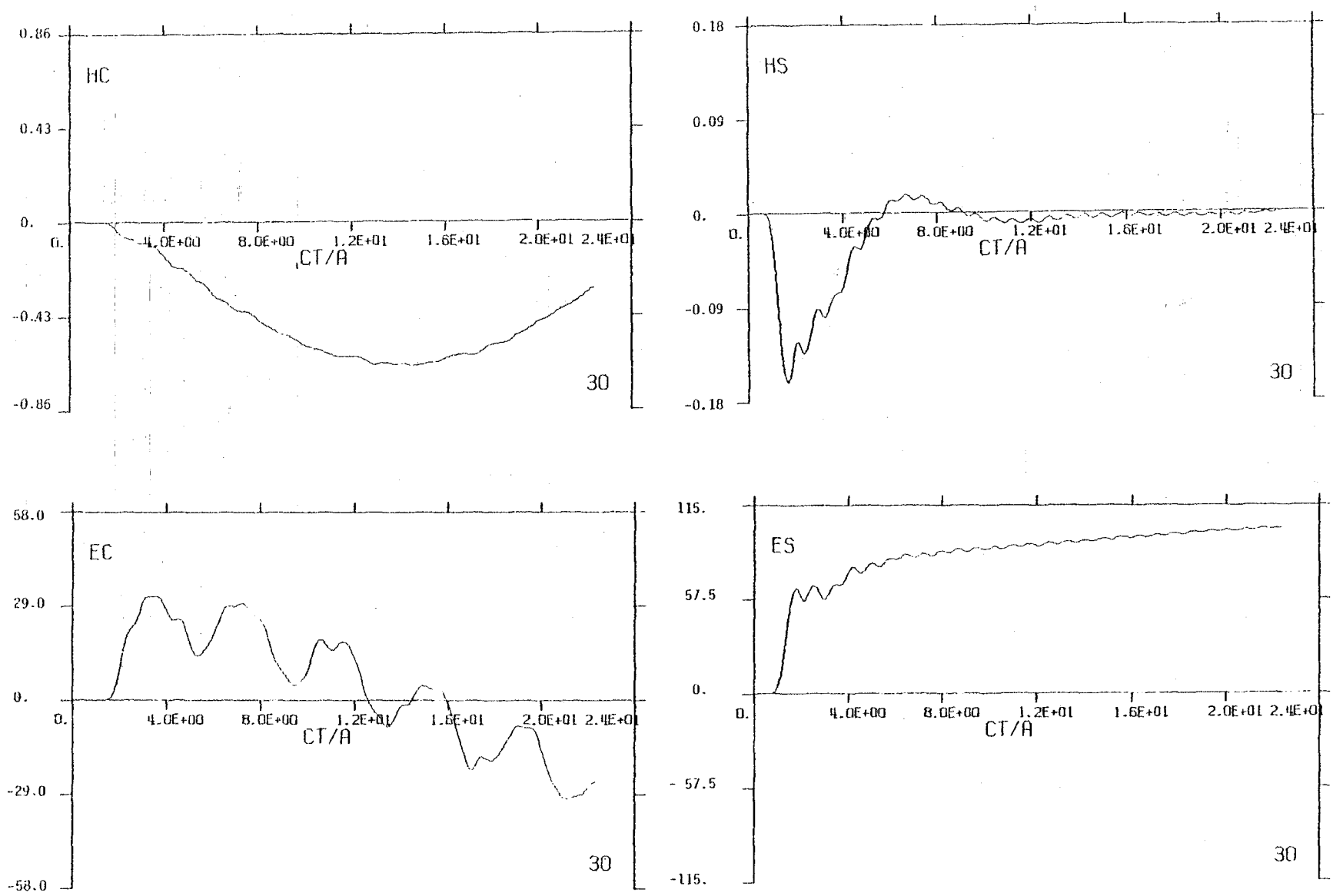

Figure 11. Cylinder Response for ρ-Directed Ring Dipole at (z/a, ρ/a) = (0.25, 0.875).

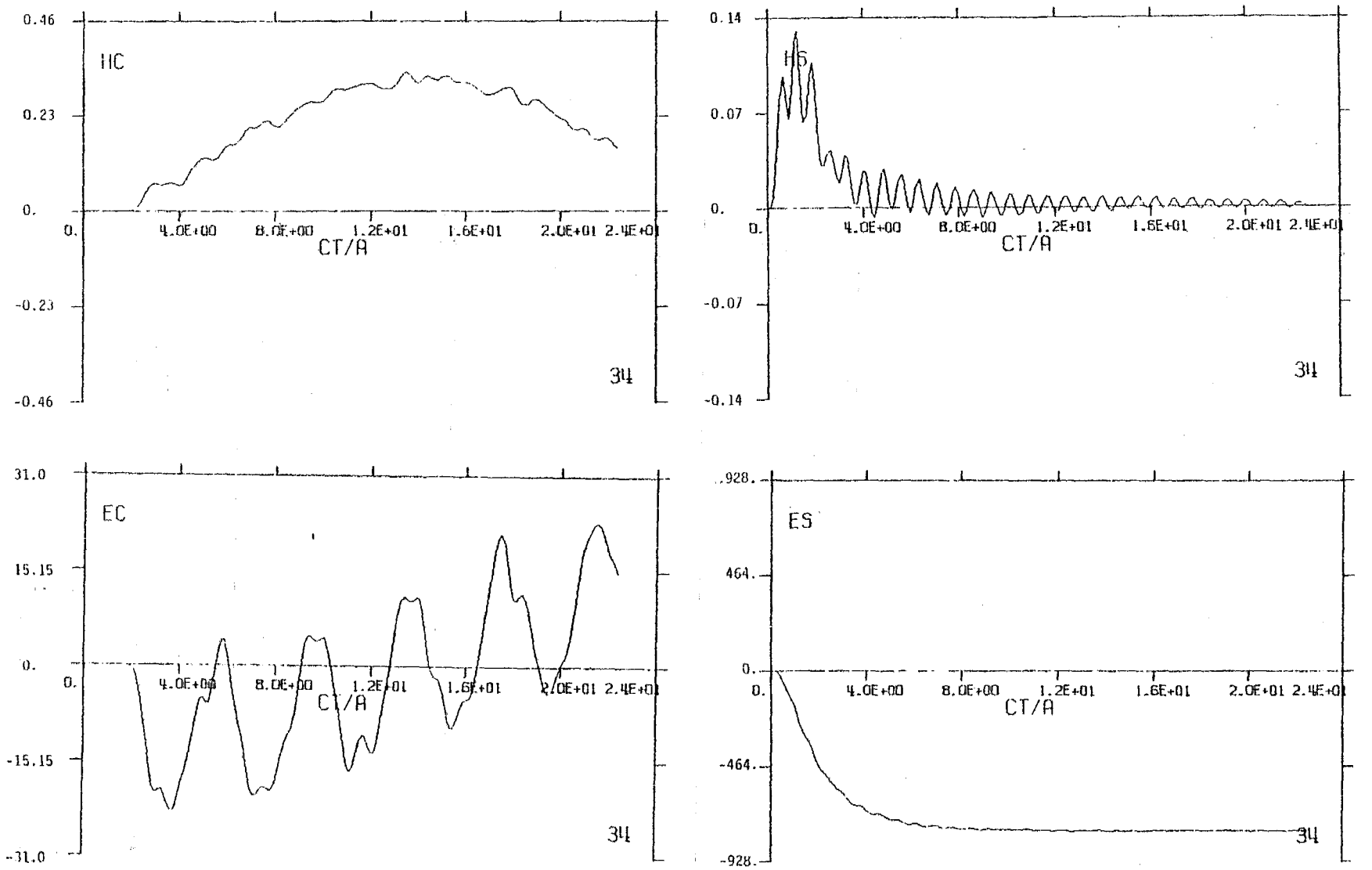

Figure 12. Cylinder Response for ρ-Directed Ring Dipole at (z/a, ρ/a) = (-1.00, 1.625).

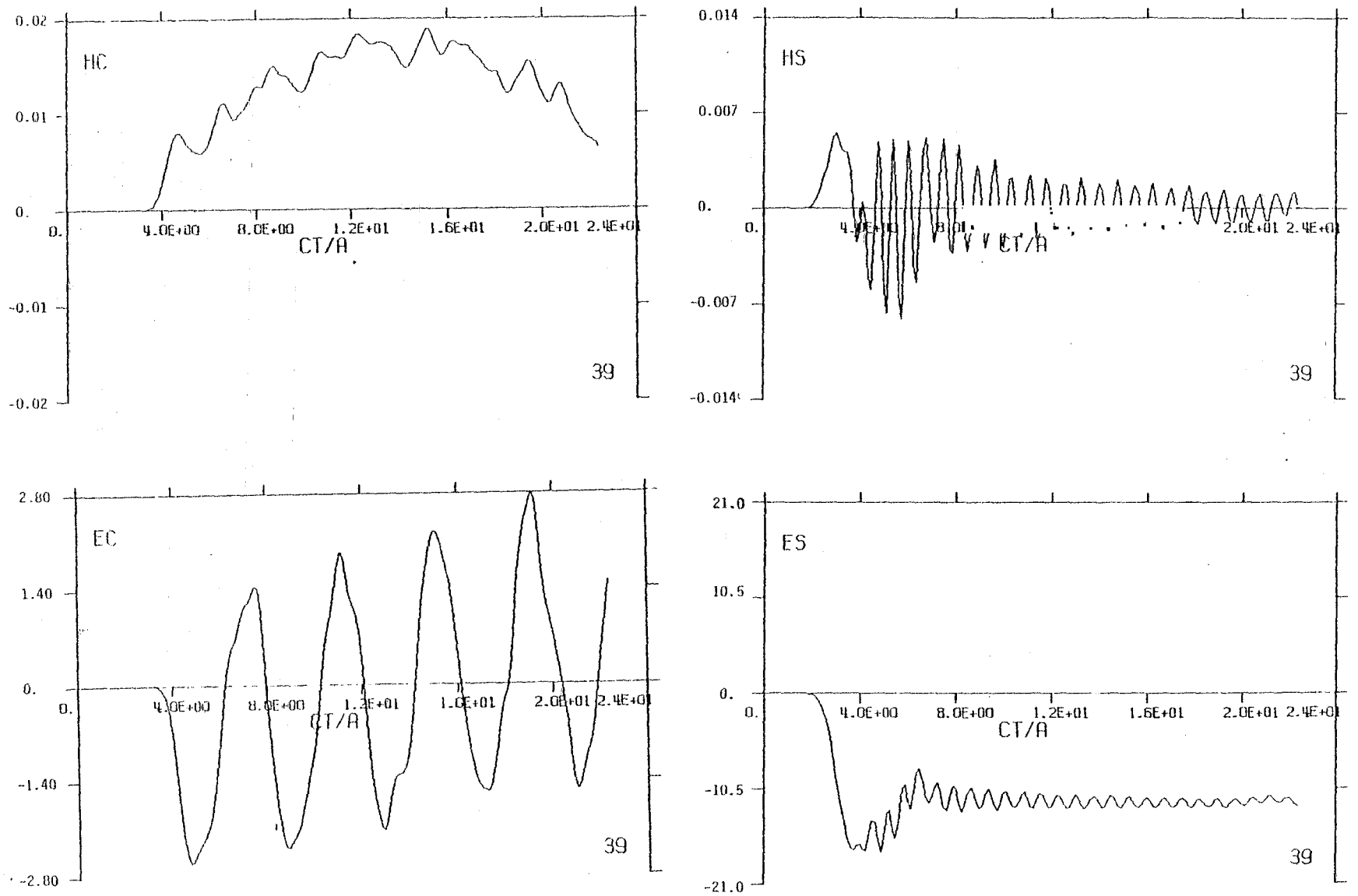

Figure 13. Cylinder Response for ρ-Directed Ring Dipole at (z/a, ρ/a) = (-1.00, 3.625).

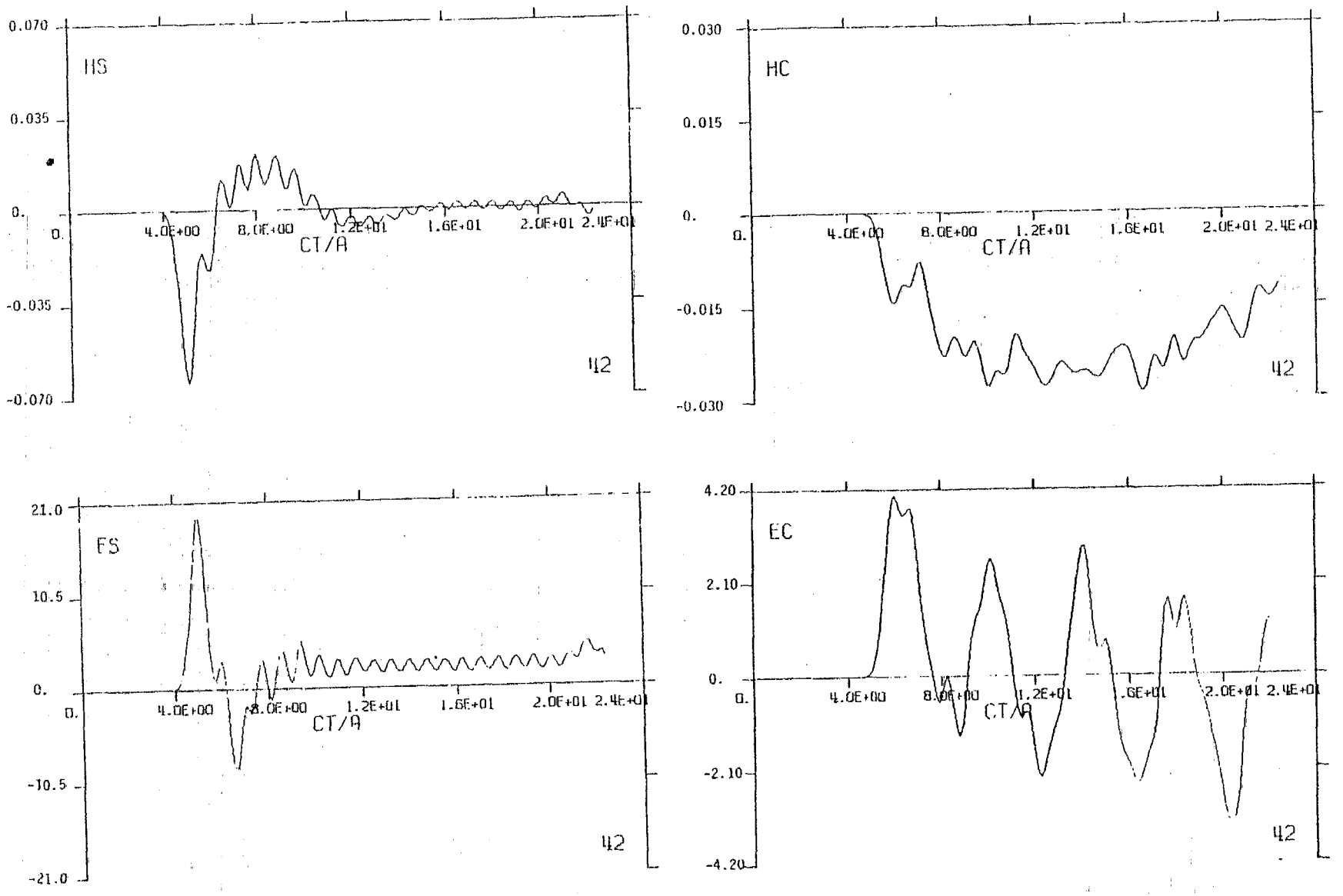

Figure 14. Cylinder Response for ρ-Directed Ring Dipole at (z/a, ρ/a) = (3.00, 3.625).

SECTION IV

CONVOLUTION OF DIPOLE RESPONSE

1. DERIVATION OF METHOD

Use of the experimental dipole measurements-calculated SGEMP volume currents will require interfacing the two sets of data and combining them to result in the predicted SGEMP system response. Below is a brief derivation of the method we can use when processing experimental pulse data. The procedure would avoid the need for first Fourier transforming, combining, and then inverse transforming back into the time domain at each antenna location. The method is now described.

For specified volume currents, it is assumed that the system's response is linearly related to the system stimulus. Letting V be the response and I be the stimulus, the relation can be expressed

$$V(t) = \int_{-\infty}^{\infty} I(\tau)K(t - \tau)d\tau \qquad (1)$$

Equation (1) can be thought of as a linear transformation from the set I to the set V with the transformation being specified by K.

Also K is the impulse response. Substitution of $I(t) = \delta(t)$ into Eq. (1) results in a response $V(t) = K(t)$.

A useful feature of Eq. (1) is that if the response $V_1(t)$ is known for a specific stimulus $I_1(t)$, then it is possible to obtain the response V(t) for a different I(t). If $I_1(t)$ is an impulse ($= \delta(t)$), then the procedure is quite straightforward. For the more general case, it is useful to apply a Fourier transform.

In several instances, it is possible to inverse transform the intermediate result directly so that the final result can be stated explicitly in the time domain. This turns out to be the case for the stimulus $I_1(t)$ we are using for the dipole volume current (the volume current on a critically damped series RLC circuit). The resulting expression is obtained below.

Direct Fourier transformation of both sides of Eq. (1) (and application of the shifting theorem) results in

$$\tilde{V}(\omega) = \tilde{I}(\omega)\tilde{K}(\omega) \tag{2}$$

where in particular

$$\tilde{K}(\omega) = \tilde{V}_1(\omega)/\tilde{I}_1(\omega) \tag{3}$$

(The tildes refer to the respective transforms.)

For a critically damped series RLC circuit, the transform of the volume current $I_1(t)$ is given by

$$\tilde{I}_1(\omega) = \int_{-\infty}^{\infty} e^{+i\omega t} \frac{t}{T} e^{(1-t/T)} u(t)dt \tag{4}$$

where $I_1(t)$ has been normalized to 1 Am at $t = T$ (the peak amplitude), $u(t)$ is the unit step, and T is the circuit time constant.

Performing the integration in Eq. (4), substitution of $\tilde{I}_1(\omega)$ into Eq. (3)

$$\tilde{K}(\omega) = \frac{1}{eT}\left[1 - 2i\omega T - \omega^2T^2\right]\tilde{V}_1(\omega) \tag{5}$$

resulting in a $K(\tau)$ (inverse transform)

$$K(\tau) = \frac{1}{eT2\pi}\int_{-\infty}^{\infty}\left[1 - 2i\omega T - \omega^2T^2\right]e^{-i\omega\tau}\tilde{V}_1(\omega)\,d\omega \tag{6}$$

$$K(\tau) = \frac{1}{e\bar{T}} \left[1 + 2T \frac{\partial}{\partial \tau} + T^2 \frac{\partial^2}{\partial \tau^2} \right] \frac{1}{2\pi} \int_{-\infty}^{\infty} e^{-i\omega\tau} \tilde{V}_1(\omega)\, d\omega \tag{7}$$

$$K(\tau) = \frac{1}{e\bar{T}} \left[V_1(\tau) + 2T \frac{\partial V_1}{\partial \tau}(\tau) + T^2 \frac{\partial^2 V_1}{\partial \tau^2}(\tau) \right] \tag{8}$$

where the inverse transform has been identified in Eq. (7). Substituting K into Eq. (1) and using a change of variable $\tau' = t - \tau$

$$V(t) = \frac{1}{e\bar{T}} \int_{-\infty}^{\infty} I(t - \tau) \left[V_1(\tau) + 2T \frac{\partial V_1}{\partial \tau}(\tau) + T^2 \frac{\partial^2 V_1}{\partial \tau^2}(\tau) \right] d\tau \tag{9}$$

For pulse application, further simplifications occur.

For $\begin{cases} \tau \leq 0, \quad V_1(\tau) = \dfrac{\partial V_1}{\partial \tau}(\tau) = 0 \quad * \\ t \leq \tau, \; I(t - \tau) = 0 \end{cases}$

The final result is**

$$V(t) = \frac{1}{e\bar{T}} \int_{0}^{t} I(t - \tau) \left[V_1(\tau) + 2T \frac{\partial V_1}{\partial \tau}(\tau) + T^2 \frac{\partial^2 V_1}{\partial \tau^2}(\tau) \right] d\tau \tag{10}$$

*The condition on V_1 is equivalent to the condition of casuality.
**Concerning units, recall that the antenna volume current $I_1(t)$ was normalized to 1 Am at peak amplitude.

A useful check is to let $I(t) = I_1(t)$. If Eq. (10) is valid, then $V(t)$ should be equal to $V_1(t)$. First recognizing that

$$V_1(\tau) + 2T \frac{\partial V_1}{\partial \tau}(\tau) + T^2 \frac{\partial^2 V_1}{\partial \tau^2}(\tau) = T^2 e^{-\tau/T} \frac{\partial^2}{\partial \tau^2}\left[e^{\tau/T} V_1(\tau)\right] \tag{11}$$

and substituting this and $I_1(t - \tau)$ into Eq. (10)

$$V(t)\Big|_{I=I_1} = e^{-t/\tau} \int_0^t (t - \tau) \frac{\partial^2}{\partial \tau^2}\left[e^{\tau/T} V(\tau)\right] d\tau \tag{12}$$

Integration of Eq. (12) by parts twice results in

$$V(t)\Big|_{I=I_1} = V_1(t) - e^{-t/T}\left[V_1(0) + \frac{t}{T}\left\{V_1(0) + T \frac{\partial V}{\partial t_1}(0)\right\}\right] \tag{13}$$

$$V(t)\Big|_{I=I_1} = V_1(t)$$

since $V_1(0)$, $\frac{\partial V_1}{\partial t}(0)$ are zero.

The numerical analog of Eq. (10) is now discussed. All operations of the convolution would be performed on a computer, that is, not a continuous integration, but a summation on a finite mesh.

The numerical analog of Eq. (10) that appears appropriate for uniform time spacing is given by

$$V^{\ell} = \frac{T}{e(dt)} \sum_{k=2}^{\ell-1} I^{\ell-k} \left[- 2V_1^k + e^{dt/T} V_1^{k+1} + e^{-dt/T} V_1^{k-1} \right] \tag{15}$$

$$\text{------} \quad V_1^{-1}, V_1^0, V_1^1, V_1^2 = 0 \tag{16}$$

where the superscripts refer to the time value

$$t = \ell * dt, \quad V(t) \rightarrow V^{\ell} \tag{17}$$

and dt is the time step. (The time has been shifted by 2*dt to avoid a negative subscript on the computer.)

It will be shown below that the numerical analog is exact when I(t) = $I_1(t)$ is substituted into Eq. (15). In terms of the finite quantities

$$I^{\ell-k} = e(\ell - k)\xi \, e^{-(\ell-k)\xi}, \quad \xi = \frac{dt}{T} \tag{18}$$

Now let $\ell = 6$ for example. Equation (15) becomes (performing the sum)

$$V^6\Big|_{I=I_1} = \sum_{k=2}^{5} (6 - k)e^{(k-6)\xi}\left[- 2V_1^k + e^{+\xi}V^{k+1} + e^{-\xi}V_1^{k-1}\right]$$

$$= \left\{ \begin{array}{l} 4\left[0 + e^{-3\xi}V_1^3 + 0 + 3 - 2e^{-3\xi}V_1^3 + e^{-2\xi}V_1^4 + 0\right] \\ \\ \quad + 2\left[- 2e^{-2\xi}V_1^4 + e^{-\xi}V^5 + e^{-3\xi}V_1^3\right] \\ \\ \quad + \left[- 2e^{-\xi}V_1^5 + V_1^6 + e^{-2\xi}V_1^4\right] \end{array} \right.$$

$$= e^{-3\xi}V_1^3\left[4 - 3(2) + 2\right] + e^{-2\xi}V_1^4\left[3 - 2(2) + 1\right] + e^{-\xi}V_1^5\left[2 - 2\right] + V_1^6$$

$$V^6\Big|_{I=I_1} = V_1^6 \qquad (19)$$

2. AN EXAMPLE

Before proceeding further, a simple test was performed to gain confidence in the method. In Fig. 15, graph No. 1 displays a critically damped current density J1 at antenna position 2, the center top of the cylinder. Graph No. 2 in the same figure is the resulting tangential magnetic field on the cylinder side, HS (Figs. 2 and 3, Section III). Graph No. 3 in Fig. 16 is the impulse response* at this location (obtained by applying the bracketed term in Eq. (15) to HS in graph No. 2). The convolution method and an assumed second current density J2, graph No. 4, results in a second magnetic field HS, graph No. 5. The test consisted of using the fields algorithm with J2, and comparing the resulting HS, graph No. 6, with the convolution result, graph No. 5. Within graphical accuracy, the results are the same. (The time shift in graph No. 5 is consistent with the numerical algorithm, Eq. (15).)

*Graph No. 3 is actually the negative of the impulse response.

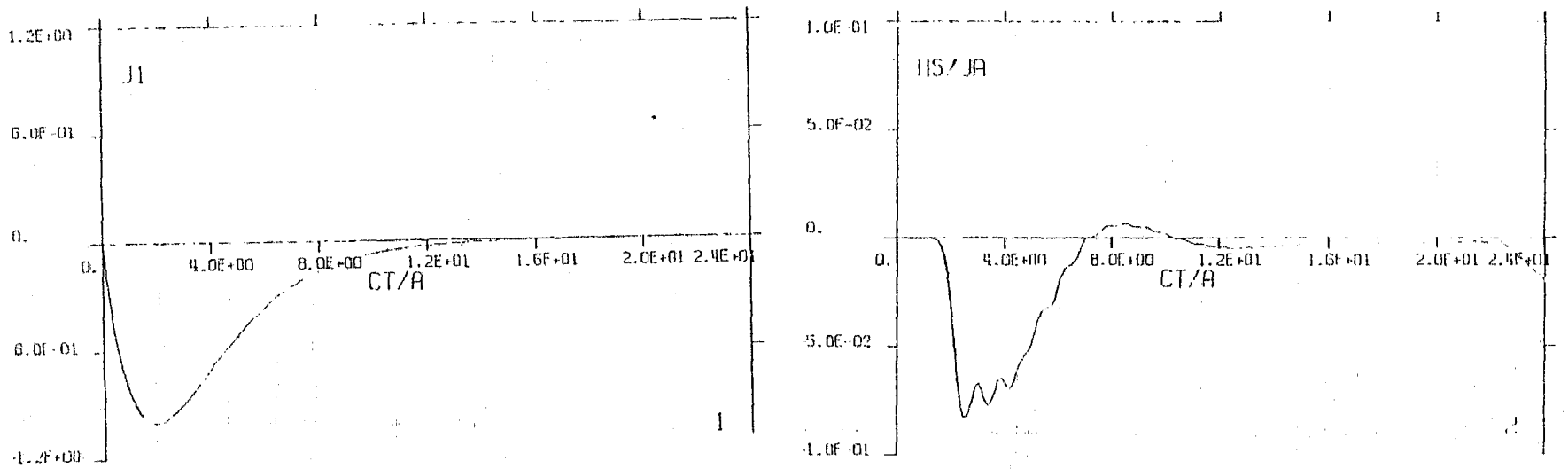

Figure 15. Convolution Method Test.

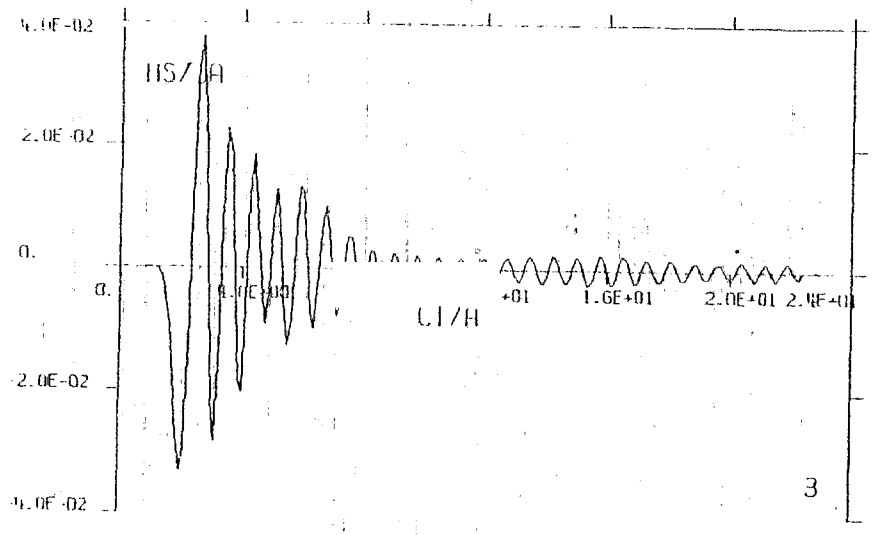

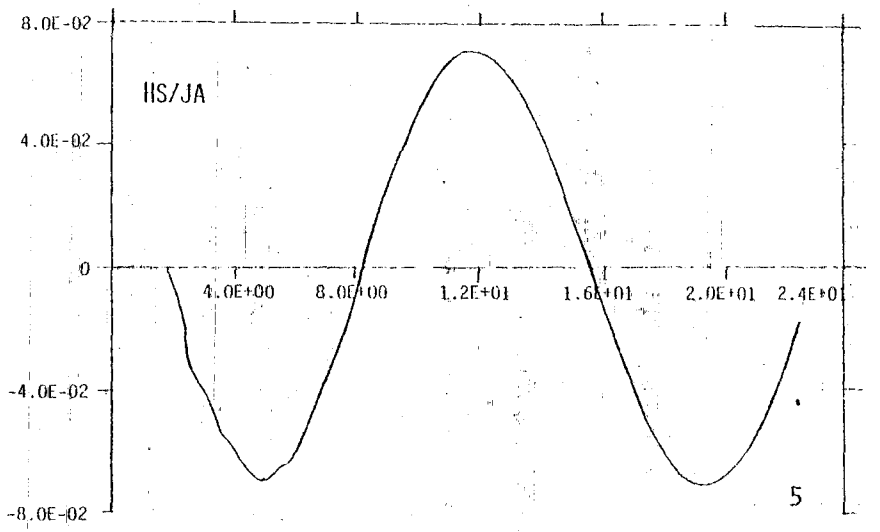

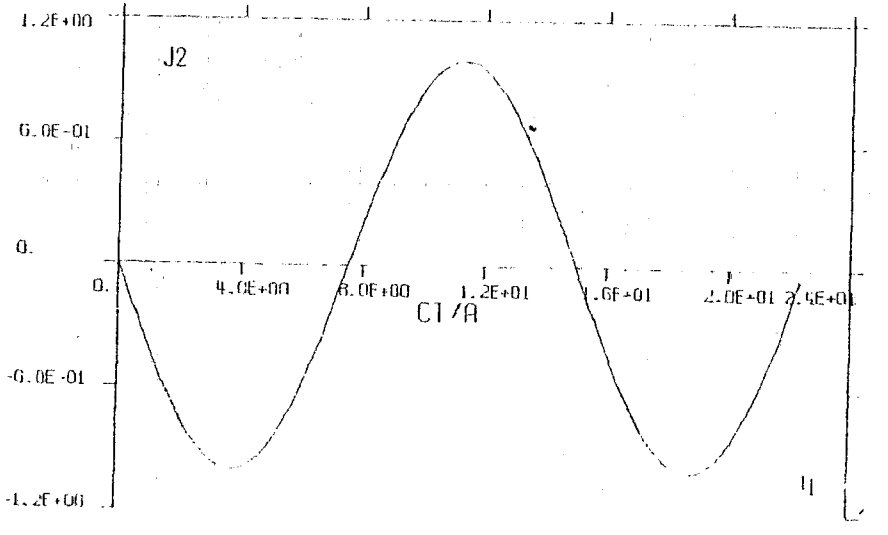

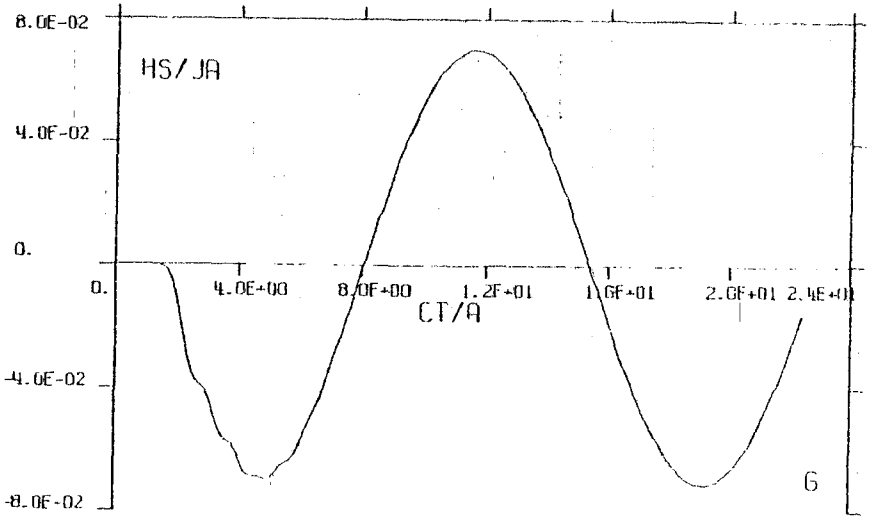

Figure 16. Convolution Method Result.

3. CONTINUOUS-WAVE DATA

In some circumstances, it would be advantageous to obtain the experimental dipole data with continuous-wave (cw) measurements, particularly whenever signal/noise is a serious problem with pulse techniques. Depending on the method, interfacing cw data with the transient SGEMP currents would require Fourier transforming, combining, and then inverse transforming back into the time domain at each antenna location. Below is a brief description of the method that appears to offer the most advantages.

Continuous-wave data would be obtained in the form of a transfer function, $T_{exp}(\omega)$, with the reference signal, amplitude, and phase, emanating from the dipole antenna. In most circumstances, the reference signal would probably be the voltage at the antenna's input terminals, V_A. For electrically small dipoles, the dipole moment P_A is linearly related to the antenna voltage

$$\frac{\partial P_A}{\partial t} = C_A h_e \frac{\partial V_A}{\partial t} \tag{20}$$

where C_A and h_e are the antenna's capacitance and equivalent electrical length, respectively. (These quantities would have to be calculated or measured for a specific antenna.) Thus, if $\frac{\partial P_A}{\partial t}$ is the desired reference for combining with the SGEMP currents, the transform of the impulse response $\tilde{K}_{exp}(\omega)$ is given by (assumed time dependence $e^{+j\omega t}$, the circumstance for most engineering hardware)

$$\tilde{K}_{exp}(\omega) = + \frac{1}{j\omega C_A h_e} T_{exp}(\omega) \tag{21}$$

$K(t)$, the impulse response, is then given by the inverse transform of $\tilde{K}_{exp}$. Once $K(t)$ is obtained, then the convolution procedure with the SGEMP currents would be the same as outlined in the previous section for pulse data.

The major advantage of the above method is that it avoids the need to Fourier transform the SGEMP currents. Furthermore, the cw data could be processed (inverse transformed) immediately into the form K(t). Thereafter, the combining of either cw data or pulse data with SGEMP currents would be the same, a distinct advantage.

Two additional considerations are worth mentioning at this point. The first is that advantage should be taken of any special symmetries that would occur in the final SGEMP scenario. For example, for end-on X-ray incidence on a cylinder, the exterior problem is independent of azimuthal angle. Thus, continuous-wave dipole data should be summed in azimuthal angle prior to inverse transforming to obtain the impulse response. This substantially reduces the amount of inverse transforming required.

Several transforming techniques are available that can be used. A major consideration is that continuous-wave data would not in general be obtained with uniform frequency steps. ABACIS, for example, has frequency steps that grow linearly with frequency.

Subroutine GFOR (on the AFWL computer), which utilizes Guilleman's technique and does not require uniform time or frequency stepping, appears to offer several advantages. It has been used extensively on other programs and is well understood. In fact, the original software for ABACIS was designed to interface with GFOR. Basic usage information follows.

SUBROUTINE GFOR USAGE INFORMATION

CALL GFOR (IND, NT, T, Y, NF, W, Z)

IND - Determines whether forward or reverse transform is done.
If IND = 0, the reverse transform is done.
If IND = 1, the forward transform is done.

NT - This is the number of time-value pairs. If the forward transform is is done, this parameter specifies the number of input values. If the reverse transform is done, this parameter specifies the number of times at which the transform is to be integrated.

T - Array containing time values for transforms.

Y - If the forward transform is done, y is the array of F(t) values. If the reverse transform is done, y is an array large enough to contain the new F(t) values.

NF - This is the number of frequencies stored in array W.

W - Array containing frequency values.

Z - Array for G(W) values. For the forward transform, z must be as large as 2*NF. For the inverse transform, Z(2N-1) contains a real values of G(W) for W(N). Z(2N) contains imaginary components of G(W) for frequency W(N).

ADDITIONAL REQUIREMENTS

COMMON/STUFF/DUM (3), TP

DUM (3) - UNUSED

TP - Contains the value $2*\Pi$.

COMMON/JF/JF(7), XM(7), CNK(7), SNK(7)

JF(7) - Array of pointers to array W which tells GFOR when Δw changes.

XM(7) - Array of Δw values corresponding to spacing in array w.

CNK - SNK - UNUSED.

Sign convention is as follows.

$$\text{Forward} \quad Z(\omega) = \int_{t_{min}}^{t_{max}} e^{-j\omega t} f(t)\, dt$$

$$\text{Reverse} \quad f(t) = \frac{1}{2\pi} \int_{0}^{W_{max}} e^{j\omega t} Z(\omega)\, d\omega$$

In the forward transform f(t) must be set to zero at T_{min} and T_{max}. In the reverse transform, there is no restriction on the values of $Z(\omega)$ at 0 and W_{max}.

4. EXPERIMENTAL CONSIDERATIONS

It will be recalled that in Eq. (10), the convolution method given is for an antenna dipole moment corresponding to the time dependence for a critically damped series RLC circuit. Referring to Eq. (10), with what appears to be relatively simple modifications, the directly recorded experimental pulse data could be K(t).

$$K(t) = \frac{1}{eT}\left\{\left[V_1(t) + T\frac{\partial V_1}{\partial t}(t)\right] + T\left[\frac{\partial V_1}{\partial t}(t) + T\frac{\partial^2 V_1}{\partial t^2}(t)\right]\right\} \qquad (22)$$

Not only would this substantially reduce the numerical processing, it should provide a significant improvement in the overall quality of the final result.

The first bracketed ([ ]) term in K(t) consists of $\frac{\partial V_1}{\partial t}$ and a constant times its time integral. The AFWL presently has the instrumentation to perform this sum directly on the experimental data for a real time pulse (with an active integrator) or for a sample time pulse (with a sample time integrator).

The second bracketed ([ ]) term is the time derivative of the first term times a constant. Development of a good electronic differentiator should not be too difficult, particularly for a sampling scope-repetitive pulser instrumentation system.

Then, for example, the first bracketed term in K(t) could be input to channel A of a dual channel sampling oscilloscope, the second bracketed term could be input to channel B. The recorded signal would then be in the A + B mode.

With this approach, the directly recorded experimental result would be $K_{exp}(t)$, with an appropriate multiplying constant for sensor sensitivity, etc. Then for a specific SGEMP scenario, the appropriate SGEMP stimulus $I_{SG}(t)$ would be used in Eq. (10) to give the predicted SGEMP response $V_{SG}(t)$.

$$V_{SG}(t) = \int_0^t I_{SG}(t - \tau)\, K_{exp}(\tau)\, d\tau \qquad (23)$$

The question of which experimental data to record is an extremely important factor affecting the overall quality of the final result. It is recommended that the hardware be developed for direct recording of the impulse response.*

*V_1 above should not be confused with voltage. For example, if B_1 is the experimental quantity of interest (Wm^{-2}), then $V_1(t) = B(t)$. If $\dot{B}$ and/or $\dot{D}$ sensors are used, the directly determined experimental quantity for pulse data would be $\frac{\partial V_1}{\partial t}$.

SECTION V

THE SGEMP CALCULATION

The SGEMP predictions in this report were made with MAD2, a computer code designed to solve two-dimensional self-consistent problems associated with systems generated electromagnetic pulse phenomena. The temporal formalism is second-order and time reversible. Cylindrical coordinates were used for all the computations. Documentation of the cylindrical version is found in Reference 3.

In the computations it was assumed that the X rays were incident on the cylinder top. The electron emission energy and angular distribution were taken to be that given in Reference 3 (nominally, the PIMBS 1A energy and angular distribution).

A Gaussian time history, full width at half-max of 6 ns, with a fluence of 0.42 Jm^{-2} (10^{-5} cal/cm^2) was assumed incident on the illuminated end of the cylinder.

The electron emission data used in the computations is given in Table 3 below. The nomenclature is that used in the MAD2 code (Reference 4).

TABLE 3

ELECTRON EMISSION DATA USED IN THE SGEMP CALCULATION

$$\frac{d^5Q}{dAdtdEd^2\Omega} = \eta s(t) f(E) \frac{1}{\pi} g(\theta)$$

E(keV)	f(E)δE (unitless)	θ(degrees)	2g(θ) sinθ (unitless)
0.9000E+00	0.2060E+00	0.1290E+02	0.1000E+01
0.1500E+00	0.2850E+01	0.2280E+02	0.1000E+01
0.2100E+01	0.2030E+00	0.3000E+02	0.1000E+01
0.2700E+01	0.1190E+00	0.3630E+02	0.1000E+01
0.3300E+01	0.3850E-01	0.4210E+02	0.1000E+01
0.3900E+01	0.3370E-01	0.4790E+02	0.1000E+01
0.4500E+01	0.2470E-01	0.5370E+02	0.1000E+01
0.5100E+01	0.2190E-01	0.6000E+02	0.1000E+01
0.5700E+01	0.1890E-01	0.6720E+02	0.1000E+01
0.6300E+01	0.1530E-01	0.7710E+02	0.1000E+01
0.6900E+01	0.9760E-02		
0.7500E+01	0.8560E-02		
0.8100E+01	0.6060E-02		
0.8700E+01	0.4030E-02		
0.9300E+01	0.3380E-02		
0.9900E+01	0.2350E-02		
0.1050E+02	0.1680E-02		
0.1110E+02	0.6640E-03		

SECTION VI

COMBINING TECHNIQUE FOR DIPOLE DATA AND SGEMP VOLUME CURRENTS

1. TIME DERIVATIVE OF SGEMP DIPOLE MOMENTS

In the computations, the space surrounding the satellite was divided into specific volume elements. At each time step in the SGEMP calculation, a sum was performed over each elemental dipole moment's time derivative occurring in a specific volume and written onto disk. At the end of the calculation, these quantities $\frac{\partial P_{SG}}{\partial t}$ (A·m) were then sorted and written back onto disk as a function of time for each volume element. These are the quantities that are used to convolve with the impulse response from a dipole antenna located at the center of the same volume.

The algorithm for storing the SGEMP dipole moment's time derivative permits changing the volume size in different regions of space. Thus, for example, small volumes in close and larger volumes farther away could be used for storing the SGEMP information without increasing the storage requirements.

The combining method consisted of the following steps.

(1) The SGEMP $\frac{\partial P's}{\partial t}$ were calculated and stored on disk.

(2) A grid detail was specified for antenna placement.

(3) Dipole data was obtained for these antenna locations (as described in Section III) and converted to the equivalent impulse response.

(4) A convolution was performed on the dipole impulse response and the total $\frac{\partial P_{SG}}{\partial t}$ for that volume of space (as described in Section IV).

(5) The procedure was continued until all the SGEMP currents were taken into account.

Results were obtained for several combinations of volume size and grid detail. The pertinent results and representative data are presented in Section VIII.

A method for taking into account the distant SGEMP currents is described in the following section.

2. FAR FIELD EFFECTS

The coupling of the more distant currents to the satellite in an SGEMP environment is not expected to be an important effect, particularly for the high fluence case. However, it is possible to include these effects with little additional effort and thereby avoid any uncertainties associated with this aspect of the simulation.

In essence, from the SGEMP calculation, the several stored dipole moments in a particular angular direction ($r > r_{\text{far field}}$) are replaced with a weighted time-shifted sum. Thus, with this method, experimental dipole far-field data is needed for only a single antenna distance in each angular interval. Generalization of the method to three dimensions would be straightforward.

To be specific, suppose that far-field experimental data is obtained at each angle θ_M, M = 1, 2, ...N, and that the distance from the antenna center to the satellite center is r_M. The far-field SGEMP volume elements K positioned at cylindrical coordinates z_K, θ_K (with respect to the satellite center) are sorted to the appropriate angular interval θ_M.

$$r_K = \sqrt{z_K^2 + \rho_K^2}$$

$$\theta_K = \tan^{-1}(z_K/\rho_K) \quad , \quad \theta_{M-\frac{1}{2}} \leq \theta_K < \theta_{M+\frac{1}{2}} \quad , \quad r_K \geq r_M$$

The r^{-1} fall off and the time delay for each SGEMP volume element are then taken into account by performing the sum*

$$\hat{r}_M \times \frac{\partial \vec{P}}{\partial t} M(t) \Big|_{\text{equiv}} = \sum_K \frac{\vec{r}_M}{r_K} \times \frac{\partial \vec{P}}{\partial t} K, SG(\tau_{MK}) \quad , \quad M = 1,2,\ldots,N$$

All K with $\theta_{M-\frac{1}{2}} \leq \theta_K < \theta_{M+\frac{1}{2}}$

$$\tau_{MK} = t - \left| r_K - r_M \right| / c$$

This quantity

$$\frac{\partial \vec{P}}{\partial t} M(t) \Big|_{\text{equiv}}$$

would then be used for the SGEMP $\frac{\partial \vec{P}}{\partial t}$ for the antenna position r_M, θ_M.

*In the far field only the transverse components contribute.

SECTION VII

GRID DETAIL/VOLUME SIZE

1. GENERAL

The volume size and grid detail required for simulation are major parameters impacting the practicality of the dipole method (DIES). The distant SGEMP currents can be taken into account by the method described in Section VI, paragraph 2 (far-field effects). Similarly, for the intermediate range antennas (~ a few satellite radii) the major consideration in grid detail appears to be the frequency content of the SGEMP currents in that region of space (this can be inferred from Section III, numerical dipole data). That is, a grid dimension should be smaller than a half wavelength for the shortest wavelength of interest.

The remaining question is the more difficult one, the requisite grid detail in the immediate vicinity of the satellite, the near field.

The techniques described earlier in this report provides the means to vary the grid detail/volume size and obtain parametric information about this constraint. For the reasons given above, the data presented in this section emphasize the conditions in the near field.

Using the calculated SGEMP currents (described in Section V) and numerical dipole data (Section III), results were obtained for several differing grid details. It soon became apparent that grid dimensions in the 10 to 20 cm range would be required in the immediate vincinity of the cylinder. For larger grid dimensions, the quality of simulation rapidly declined.

The procedure for comparison was as follows. In the SGEMP calculation, the surface tangential magnetic and normal electric fields were calculated and retained.* Using a specific grid, numerical dipole results were then convolved with the SGEMP currents and the resulting surface fields were compared to those obtained in the SGEMP calculation.

*The circumferential gap in the cylinder was closed during this series of comparisons.

No single parameter was found (at least that could be directly calculated from the data) that provided a measure of the quality of simulation. Rather, the procedure was to compare the fields at several locations on the cylinder surface as described above.*

Representative data for some cases of interest are described below. For ease of comparison, in each case the data given is for the tangential magnetic field on the cylinder side, HS.

*In the future, some thought should be given to defining a single, global parameter that can be used as a measure of the quality of simulation.

2. RESULTS

Figures 17 through 22 display representative data obtained for differing grid detail of antenna placement. The quantity given is HS (Table 2, Section III).

Figure 17 is the result obtained from the SGEMP calculation (described in Section VI). The time scale is normalized to the speed of light and the cylinder radius (0.45 m).

Figure 18 is the result obtained from convolving the SGEMP currents with antenna responses. Small ring dipoles (both polarizations) were positioned in each of the cells shown in the inset. That is, the antenna grid was 11.25 cm by 11.25 cm.

Comparing Fig. 17 and 18, it appears that the method works very well for a sufficiently fine antenna grid. The peak amplitudes agree to within approximately 5%.

In Fig. 19, the antenna grid dimensions were doubled (22.5 cm by 22.5 cm). As is evident in the figure, the peak amplitude is down approximately 20% from the direct SGEMP result.

In the next figure, Fig. 20, a varying grid size was tried, small cells in close and large cells farther away. It is evident that this choice is not an improvement over the 22.5 cm grid.

In Fig. 21, the number of antennas were doubled immediately on top of the cylinder. This resulted in some improvement in the peak value.

In Fig. 22, an 11.25 cm grid immediately adjacent to the cylinder and a 22.5 cm grid was used for the remainder of the locations. Comparing to Fig. 17, this choice appears to offer a reasonable compromise between the number of antennas in the near field and the quality of simulation.

The grid shown in Fig. 22 is not an optimized grid. For one radius or farther away from the cylinder, the antennas can be positioned slightly farther apart than shown without serious degradation in quality. However, it should be apparent that not much variation is required to substantially (>10%) change the result.

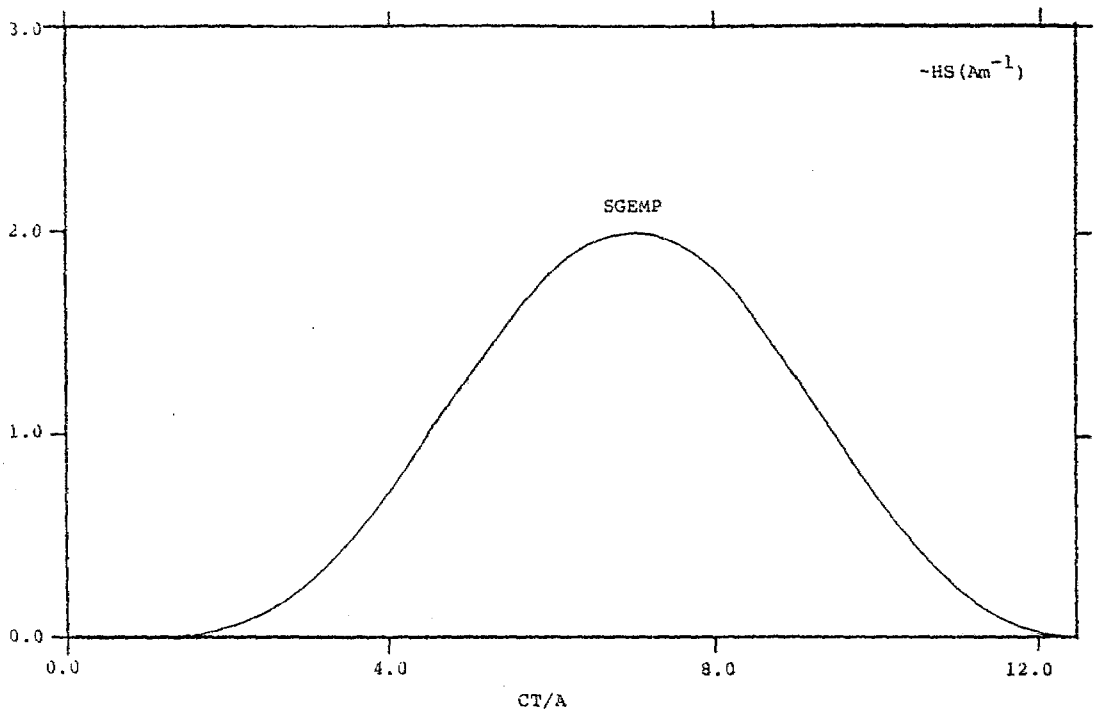

Figure 17. Cylinder Response Obtained from the SGEMP Calculation.

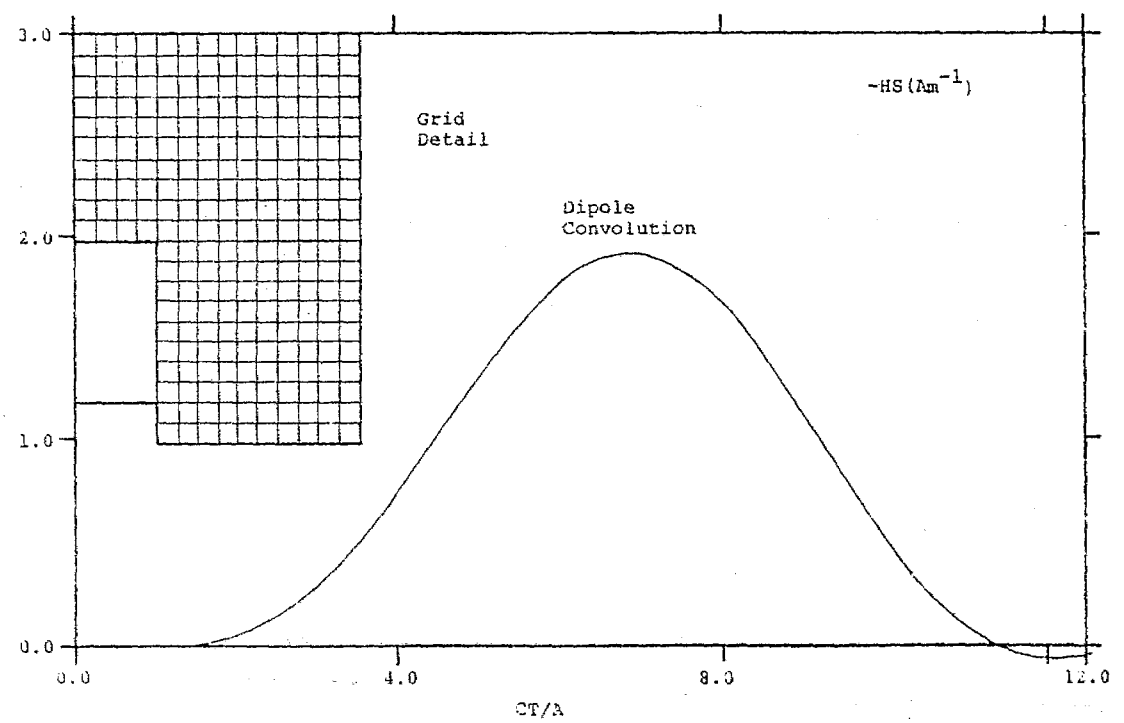

Figure 18. Cylinder Response Obtained from Convolution with a 11.25 cm Grid.

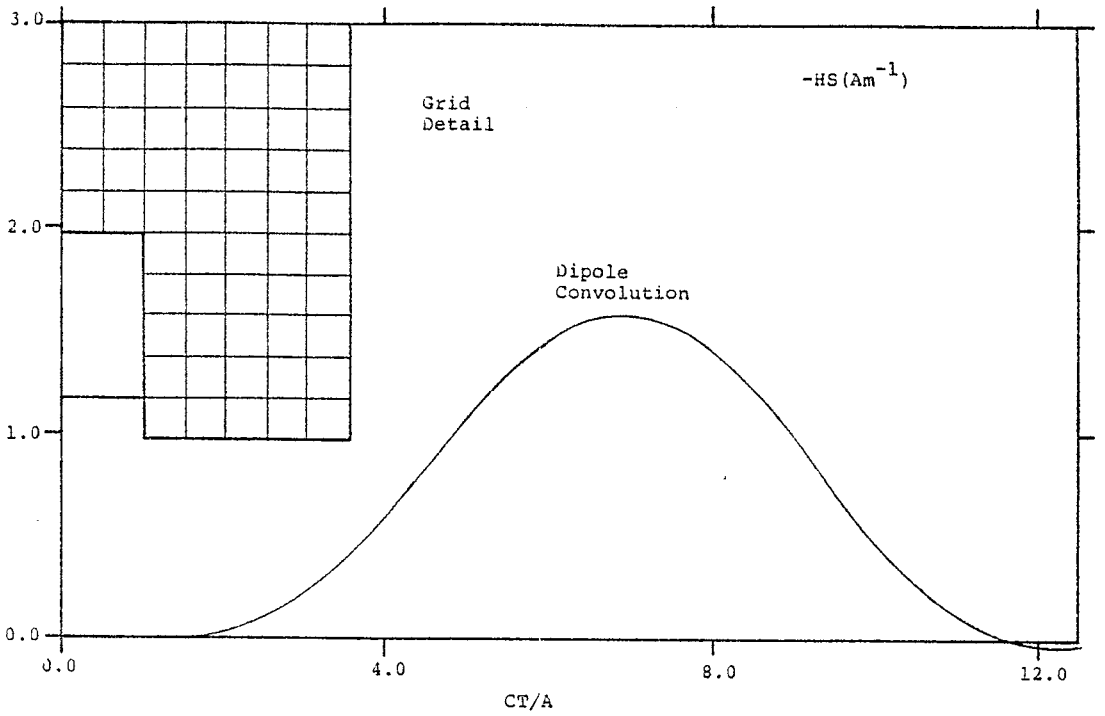

Figure 19. Cylinder Response Obtained from Convolution with a 22.5 cm Grid.

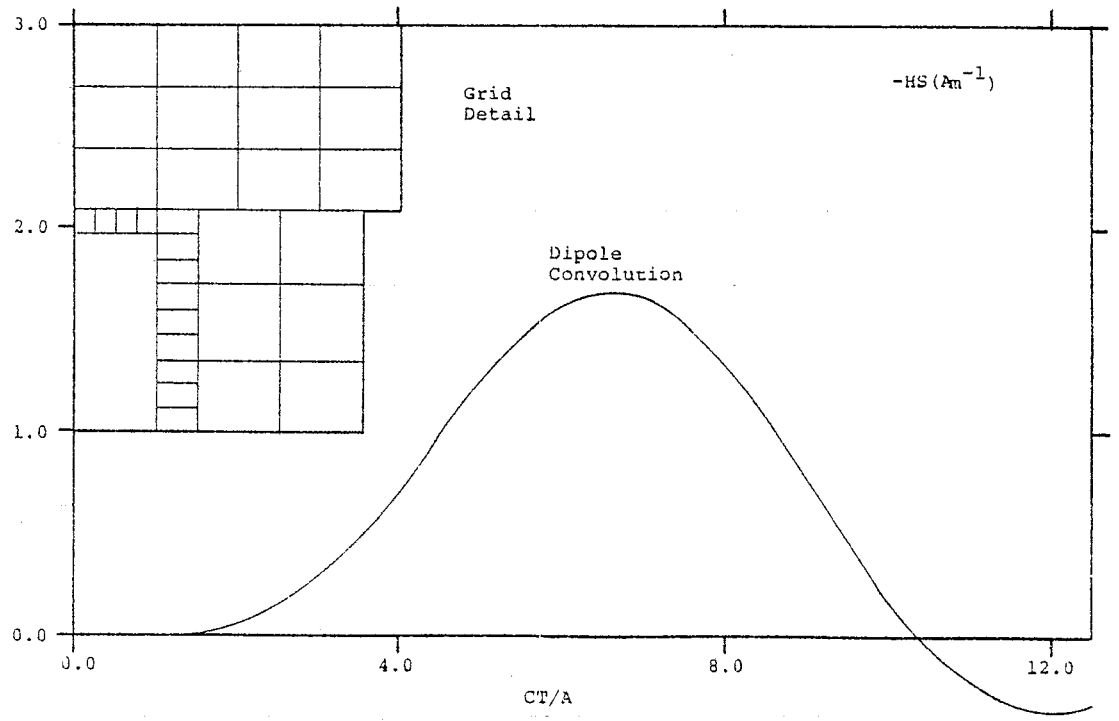

Figure 20. Cylinder Response Obtained from Convolution with a Varying Grid.

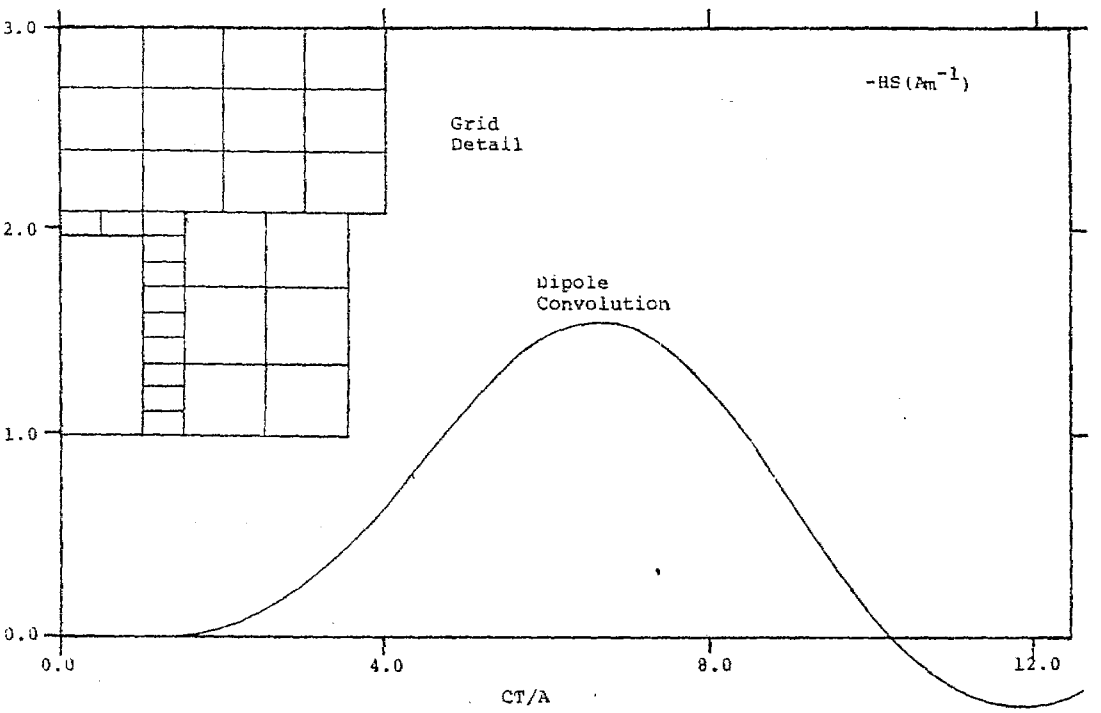

Figure 21. Cylinder Response Obtained from Convolution with a Varying Grid.

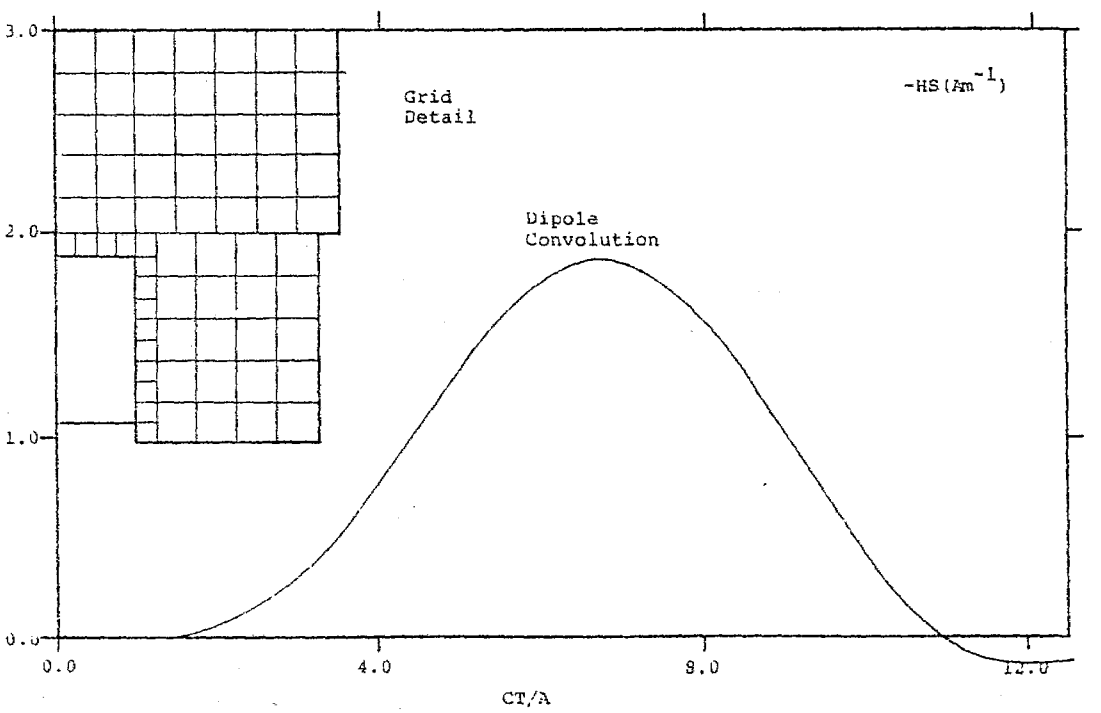

Figure 22. Cylinder Response Obtained from Convolution with a Varying Grid.

Although not conclusive, it is suggested that the requisite fineness of antenna grid positions is due to the substantial static-like coupling ($1/r^3$) of the dipoles to the satellite and to the nature of the SGEMP currents.

The bulk of the SGEMP currents travel at a speed that is slow compared to the speed of light. For example, a 10 keV electron has a velocity approximately one-fifth the speed of light. Thus, even though the current's time history may be slowly varying, the apparent center of a local SGEMP dipole moment is not well approximated by the center point of a large grid.

In particular, half-dipoles directly connected to the satellite would be desirable for the first layer of measurements.

A simple method was available for assessing the importance of the time variation of the SGEMP currents concerning grid detail in the near field. Figure 23 displays the SGEMP result for a much slower time history X-ray source (the PIMBS-1A time history, Reference 3).

Figure 24 is the convolution result for an antenna placement grid as indicated. It exhibits excellent agreement with the calculated SGEMP result (Fig. 23).

Figure 25 is the convolution result for a 22.5 cm by 22.5 cm antenna grid. Comparing this result to Fig. 23, it is apparent that the quality of simulation is substantially reduced by the larger grid.

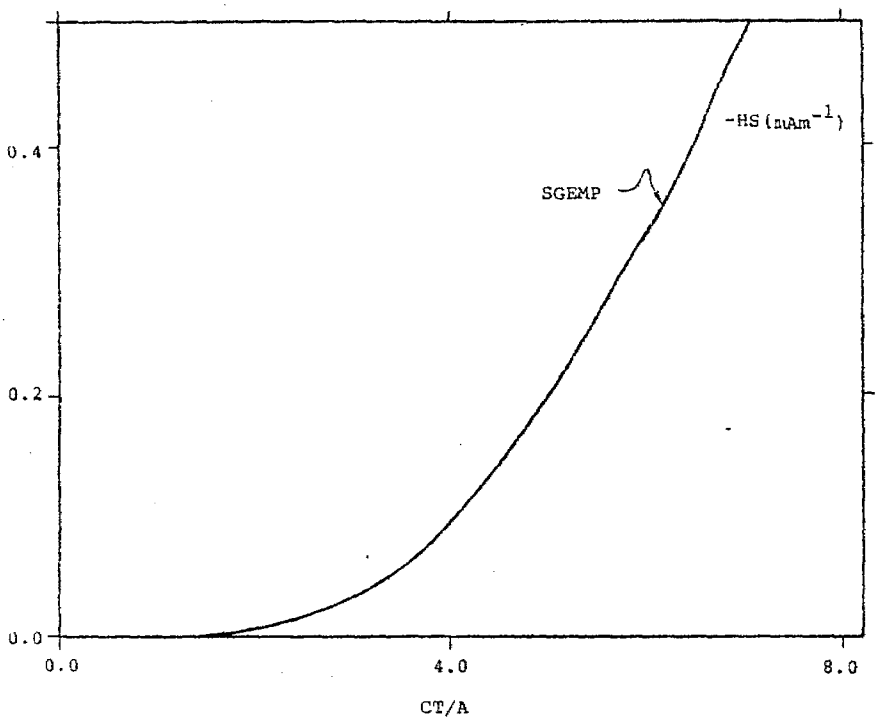

Figure 23. Cylinder Response from the SGEMP Calculation with a Slowly Varying Source.

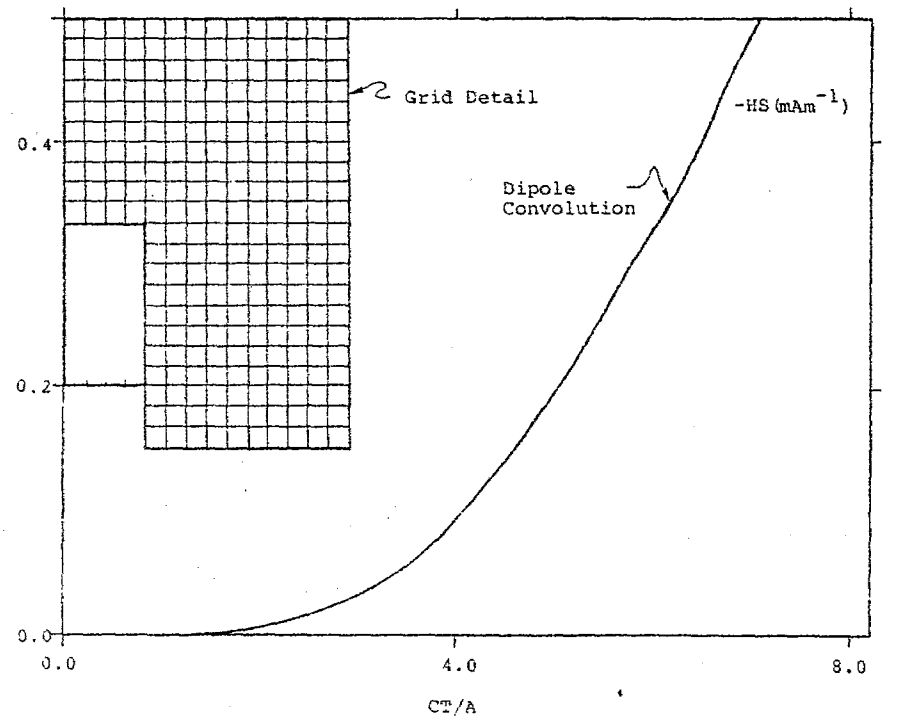

Figure 24. Cylinder Response Obtained from Convolution with a 11.25 cm Grid.

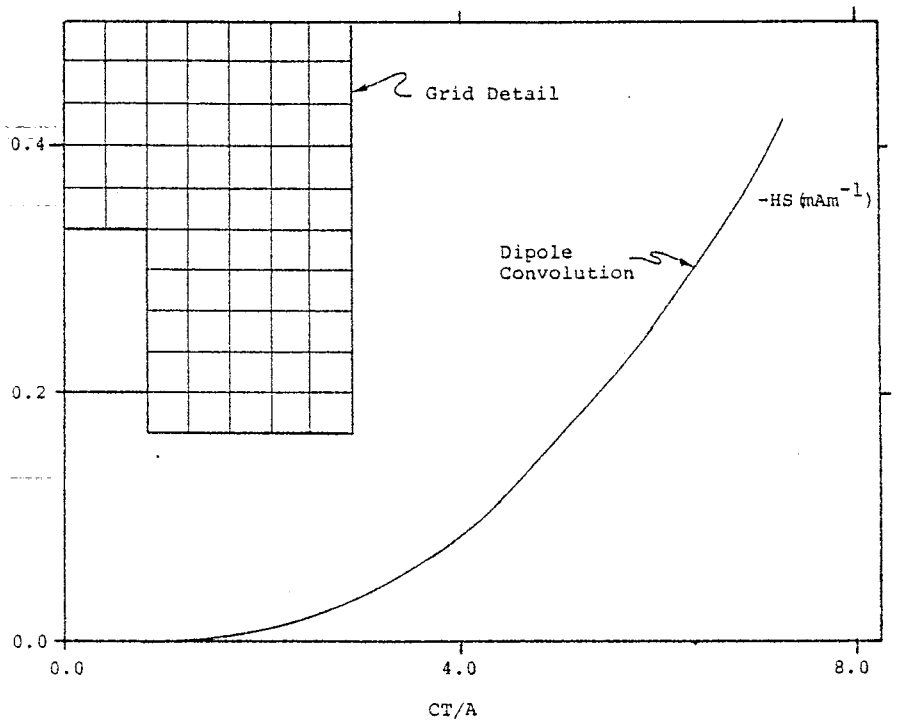

Figure 25. Cylinder Response Obtained from Convolution with a 22.5 cm Grid.

3. SUMMARY

The grid detail for antenna placement in the near field shown in Fig. 22 appears to offer a reasonable compromise between grid detail and quality of simulation. The grid shown is not an optimized grid, but is a reasonable compromise.

Requisite grid detail in the near field appears to be dominated by strong static coupling and by the fact that the currents move slowly compared to the speed of light. Half-dipoles are needed in the measurements for the layer adjacent to the satellite.

SECTION VIII

CONCLUSIONS

1. GENERAL

Results impacting the dipole method (DIES) are summarized in this section. Conclusions are presented, followed by recommendations.

Measurements were not available for testing the problems associated with combining the experimental and analytical data. As a consequence, direct time stepping of Maxwell's equations in two dimensions was used to numerically simulate the experimental dipole data.

For simplicity, the test object (described in Section II) and the analysis method (Section III) are two dimensional. The numerical method for obtaining dipole data is described in Section III. Results in that section may be retained for comparison to experimental data.

The results given for antenna position 2 (Table 1 and Fig. 4) would be the simplest comparison since for this case the excitation is aximuthally symmetric. For the other antenna positions, the tangential magnetic and normal electric fields on the exterior of the cylinder (HS, ES) must be interpreted as the azimuthally symmetric part of the cylinder response. The results given are to be compared to a sum in azimuth of the experimental cylinder response, or equivalently, a sum in azimuth over a specific antenna location (z,ρ).

A method for convolution of the dipole response that offers several advantages is described in Section IV. A technique for processing experimental continuous-wave data is described in that section. The major features of the combining techniques for dipole data and SGEMP currents are summarized in Section VI. A method is given for including far field effects.

Results obtained concerning requisite grid detail in the near field of the satellite are summarized in Section VII.

2. CONCLUSIONS

The method works. Figure 22 (Section VII) displays an antenna grid detail that offers a reasonable compromise between the number of antennas in the near field and the quality of simulation (an 11.25 cm by 11.25 cm grid adjacent to the cylinder, a 22.5 cm by 22.5 cm grid in the remainder of the near field).

Distant SGEMP currents can be accounted for by the method described in Section VI, paragraph 2.. The recommended convolution method is presented in Section IV.

3. RECOMMENDATIONS

The method shows potential for obtaining reliable information concerning SGEMP effects on a satellite. This includes consideration of several of the major practical constraints in both obtaining the experimental data and combining with the calculated SGEMP results.

Consideration should be given to replacement of the bulk of the volume currents by an equivalent surface current layer (Reference 5). Use of this method could substantially reduce the number of required antenna positions. Techniques for doing this and the effects on the quality of simulation are being examined by the author.

A parallel effort is recommended. Analysis should not be carried too far until real experimental data is processed by the procedure.

Instrumentation is not presently available for obtaining reliable experimental data. This is due mainly to the need to electrically isolate the dipoles for the close in measurements and to maintain a phase or time reference. Developmental effort would be required, less effort would be needed to obtain experimental pulse data. Effort should be directed towards constructing a small self-contained pulse-driven dipole (and a

small half-dipole). The critically damped antenna current described in this report offers several advantages. Construction of the hardware to obtain the equivalent impulse response is recommended.

A more realistic satellite geometry should be addressed in the analysis. Results on the simplified model in this report justify going to a three-dimensional object with electronic circuitry in the interior. Since the method works, internal data of real interest could be obtained in a first experiment.

REFERENCES

1. Baum, C. E., "Some Types of Small EMP Simulators," Miscellaneous Simulator Memos, Memo 9, 22 December 1976.

2. Baum, C. E., "EMP Simulators for Various Types of Nuclear EMP Environments: An Interim Categorization," adapted from AFWL SSN 151 and also published in the Special Joint Issue on the Nuclear Electromagnetic Pulse, IEEE Trans. on Antennas and Propagation, January 1978 and IEEE Trans. on Electromagnetic Compatibility, February 1978.

3. Fishbine, B., B. Goplen, R. E. Clark and G. Seely, "Two- and Three-Dimensional Calculations for the PIMBS 1A Cylinder Experiment, Theoretical Note 291, February 1977.

4. Goplen, B., R. Clark and B. Fishbine, "MAD2 - A Computer Code for System-Generated Electromagnetic Pulse (SGEMP) Calculations in Two Dimensions," Theoretical Note 290, January 1977.

5. Harrington, R. F., Time Harmonic Electromagnetic Fields, McGraw-Hill, 1961, pp. 106-110.